1998

Metallic photonic band gap structures on flexible substrates

Sandhya Gupta
Iowa State University

INFORMATION TO USERS

This manuscript has been reproduced from the microfilm master. UMI films the text directly from the original or copy submitted. Thus, some thesis and dissertation copies are in typewriter face, while others may be from any type of computer printer.

The quality of this reproduction is dependent upon the quality of the copy submitted. Broken or indistinct print, colored or poor quality illustrations and photographs, print bleedthrough, substandard margins, and improper alignment can adversely affect reproduction.

In the unlikely event that the author did not send UMI a complete manuscript and there are missing pages, these will be noted. Also, if unauthorized copyright material had to be removed, a note will indicate the deletion.

Oversize materials (e.g., maps, drawings, charts) are reproduced by sectioning the original, beginning at the upper left-hand corner and continuing from left to right in equal sections with small overlaps. Each original is also photographed in one exposure and is included in reduced form at the back of the book.

Photographs included in the original manuscript have been reproduced xerographically in this copy. Higher quality 6" x 9" black and white photographic prints are available for any photographs or illustrations appearing in this copy for an additional charge. Contact UMI directly to order.

UMI

A Bell & Howell Information Company
300 North Zeeb Road, Ann Arbor MI 48106-1346 USA
313/761-4700 800/521-0600

Metallic photonic band gap structures on flexible substrates

by

Sandhya Gupta

A dissertation submitted to the graduate faculty

in partial fulfillment of the requirements for the degree of

DOCTOR OF PHILOSOPHY

Major: Electrical Engineering (Microelectronics)

Major Professor: Gary Tuttle

Iowa State University
Ames, Iowa

1998

Graduate College
Iowa State University

This is to certify that the Doctoral dissertation of

Sandhya Gupta

has met the dissertation requirements of Iowa State University

Signature was redacted for privacy.

Major Professor

Signature was redacted for privacy.

For the Major Program

Signature was redacted for privacy.

For the Graduate College

TABLE OF CONTENTS

Metallic photonic band gap structures on flexible substrates

by

Sandhya Gupta

Major Professor: Gary Tuttle

Iowa State University

Periodic dielectric and metallic structures have recently generated great interest because they can exhibit a forbidden range of frequency, or a photonic band gap (PBG) where the electromagnetic waves cannot propagate. Since their theoretical prediction in 1987, several applications at frequencies ranging from microwave to optical region have been proposed using these novel structures. This presentation demonstrates the first successful fabrication of flexible metallic PBG structures that show frequency filtering properties at far-infrared frequencies.

The metallic PBG filters described here are multi-layered metallic meshes imbedded in a flexible polyimide dielectric. They have a simple, microfabrication-based construction that use alternating dielectric and metal layers and result in structures that are mechanically flexible. Depending on the periodic pattern of the metal grids, the filters have either simple high-pass, band stop or a more a complex transmission characteristic. The critical frequencies of the filters depend on the spatial periodicity of the metal grids and the inter-layer separation. The transmission characteristic of these filters show cut-off frequencies in the far-infrared region with very high attenuation (>35 dB) and large fractional bandwidths.

The measured values are in very good agreement with theoretical results. The filters maintain their optical characteristics after repeated bending, demonstrating mechanical

robustness of the metallic PBG structure. Rapid cooling of the samples in liquid nitrogen also does not show any visible stress on the sample or its optical characteristics making them excellent candidates for space applications.

I. INTRODUCTION

I.1 Idea of Photonic Band Gaps

Photonic band gap (PBG) structures are periodic dielectric structures that exhibit frequency regions in which electromagnetic waves cannot propagate. The idea for PBGs was first proposed by Eli Yablonovitch in 1987 [1]. The interest in PBGs arises from the fact that photon behavior in a dielectric structure is similar to the behavior of electrons in a semiconductor. The periodic arrangement of atoms in a semiconductor lattice opens up forbidden gaps in the energy band diagram for the electrons. Similarly in PBG structures, the periodic placement of dielectric "atoms" opens up forbidden gaps in the photon energy bands. This analogy can be easily seen in the Schrödinger equation (1) of a propagating electron wave in a potential, $V(\mathbf{r})$ and equation (2), which is derived from the Maxwell's equations, for the electric field amplitude $\mathbf{E}(\mathbf{r})$ propagating a monochromatic electromagnetic wave of frequency ω in an inhomogeneous but nondispersive dielectric media as shown in the following equations

$$\left\{-\frac{h^2}{2m}\nabla^2 + V(\mathbf{r})\right\}\psi(\mathbf{r}) = E\psi(\mathbf{r}). \tag{1}$$

$$-\nabla^2\mathrm{E}(\mathbf{r}) + \nabla(\nabla\cdot\mathrm{E}(\mathbf{r})) - \frac{\omega^2}{c^2}\varepsilon_{fluc}(\mathbf{r})\mathrm{E}(\mathbf{r}) = \varepsilon_o\frac{\omega^2}{c^2}\mathrm{E}(\mathbf{r}). \tag{2}$$

Here, m is the electron rest mass and $\psi(\mathbf{r})$ is the scalar wave function in equation (1). In equation (2), the total dielectric is separated as

$$\varepsilon(\mathbf{r}) = \varepsilon_o + \varepsilon_{fluc}(\mathbf{r}), \tag{3}$$

where ε_o is the average dielectric constant value and $\varepsilon_{fluc}(\mathbf{r})$ defines the spatially fluctuating part.

The latter plays a role analogous to the $V(\mathbf{r})$ in the Schrödinger equation, and the quantity $\varepsilon_o \omega^2/c^2$ is equivalent to the energy eigenvalue E of the Schrödinger equation.

The idea of PBGs has led to the proposal of many novel applications [2] at optical wavelengths, such as thresholdless lasers, single-mode light-emitting-diodes and optical wave guides. In addition, PBGs are already being used in the millimeter and microwave regimes, where the applications include efficient reflectors, antennas, filters, sources and waveguides. They have also found possible applications as infrared filters. As a result, they have been extensively studied in the last few years.

The PBG structures behave as ideal reflectors in the band gap region. Depending on the directional perdiocity of these dielectric structure, the band gap may exist in 1-D, 2-D or all the three directions.

I.2 Properties of Photonic Band Gap Structure

I.2.1 Scaleable

One of the unique features of PBG structures is their scaleable characteristic from microwaves to optical frequency[3]. This can be explained better by going back to Maxwell's equations. Equation (2) listed earlier is derived from Maxwell's equations which can be rewritten in a magnetic field vector form as:

$$\nabla \times \left(\frac{1}{\varepsilon(\mathbf{r})} \nabla \times \mathrm{H}(\mathbf{r}) \right) = \left(\frac{\omega}{c} \right)^2 \mathrm{H}(\mathbf{r}), \tag{4}$$

where $\mathbf{H}(\mathbf{r})$ is the magnetic field vector. Lets define a new dielectric constant,

$$\varepsilon'(\mathbf{r}) = \varepsilon(\mathbf{r}/s) = \varepsilon(\mathbf{r}') \tag{5}$$

where s is some scalar parameter. We have basically compressed or expanded the dielectric by this scalar value s. Now defining a new variable, $\mathbf{r}' = s\mathbf{r}$ and $\nabla' = \nabla/s$, we can rewrite equation (4) as:

$$s\nabla' \times \left(\frac{1}{\varepsilon(\mathbf{r}'/s)} s\nabla' \times H(\mathbf{r}'/s) \right) = \left(\frac{\omega}{c} \right)^2 \times H(\mathbf{r}'/s) \tag{6}$$

which can also be written as

$$\nabla' \times \left(\frac{1}{\varepsilon'(\mathbf{r}')} \nabla' \times H(\mathbf{r}'/s) \right) = \left(\frac{\omega}{cs} \right)^2 \times H(\mathbf{r}'/s) \tag{7}$$

Here, $\varepsilon(\mathbf{r}'/s) = \varepsilon'(\mathbf{r}')$ and this gets us back to the master equation with mode profile $H'(\mathbf{r}') = H(\mathbf{r}'/s)$ and frequency $\omega' = \omega/s$. If we want to study the mode profile after changing the length scale by a factor of s, we just need to scale the old mode and its frequency by the same factor. The solution of a problem at one length scale determines the solutions at all other scales.

The modes of photonic crystals can be tested at microwave frequencies with bigger dimension and because of scalability of the structure we can ensure that the electromagnetic properties will not change at optical frequencies with submicron dimensions.

Now studying the effect of change in the dielectric configuration, suppose that a new system has a dielectric constant $\varepsilon'(\mathbf{r}) = \varepsilon(\mathbf{r})/s^2$. Therefore,

$$\nabla \times \left(\frac{1}{s^2 \varepsilon'(\mathbf{r})} \nabla \times \mathbf{H}(\mathbf{r}) \right) = \left(\frac{\omega}{c} \right)^2 \times \mathbf{H}(\mathbf{r}) \tag{8}$$

or,

$$\nabla \times \left(\frac{1}{\varepsilon'(\mathbf{r})} \nabla \times \mathbf{H}(\mathbf{r}) \right) = \left(\frac{s\omega}{c} \right)^2 \times \mathbf{H}(\mathbf{r}) \tag{9}$$

The harmonic modes of the system are unchanged but all the frequencies have been scaled up by a factor of *s*. For example, if we multiply the dielectric constant by a factor of 1/4, the mode patterns are unchanged but the frequencies are doubled. So, by changing the dielectric constant or changing the dimensions of the structure, the electromagnetic properties can be scaled anywhere from microwave to optical frequencies.

I.2.2 Defect Modes

Similar to the impurity doping in a semiconductor, localized electromagnetic modes can be created in the bandgap region of PBG structures by introducing defects that disturb the periodicity of the structure [5]. This can be achieved by adding extra material to the crystal, which acts like a donor atom of a semiconductor. The defect gives rise to donor modes which have their origin at the bottom of the conduction band. A defect can also be introduced by removing a part of the material, thus creating states similar to the semiconductor behavior with acceptor atoms. Experiments have shown that the acceptor modes, acting like cavities, are of greater importance with their highly localized and single-mode cavity characteristics. In photonic crystals with defects, the transmission spectrum is changed by the presence of a narrow transmission peak within the band gap. Defect peaks with quality factors in the range of 1000-2000 have been experimentally demonstrated.

I.3 Metallic Photonic Band Gap Structures

Much of the PBG research effort has focused on the use of purely dielectric material. Metallic photonic band gap (MPBG) structures have received relatively little attention due to perceived problems relating to lossiness in the metal components.

However, MPBG structures do have some distinct advantages over their dielectric counterparts, and these advantages have garnered MPBGs more attention recently [5-7]. MPBG structures offer the potential of lighter weight, reduced size and lower materials and fabrication costs when compared to dielectric structures. The use of metal can also lead to fundamentally different PBG characteristics. For an interconnected mesh structure, the stop bands of the MPBG will extend from zero frequency up to some cut-off frequency, which is determined by the periodicity of the structure. Such behavior is in contrast to purely dielectric PBG structures, which typically have stop bands extending over relatively narrow ranges of frequencies. On the other hand, it has also been shown that MPBG structures consisting of isolated metal patches have a band-stop behavior very similar to the dielectric photonic band gap structures [8].

The MPBG structures described in this work are related to frequency selective surfaces (FSSs), which are two dimensional arrays of metallic patches or aperture elements that have frequency-filtering properties. Frequency selective surfaces have been studied in great detail [9-11] because of their application as filters, bandpass radomes, polarizers and mirrors in microwave region. Most of the fabrication work on frequency selective surfaces has focused on single-layer metal patterns.

I.4 Major Contributions

This work demonstrates successful design, fabrication and characterization of MPBG-based filter structures operating at far-infrared frequencies. The MPBGs have a simple, microfabrication-based construction that uses alternating dielectric and metal layers and results in structures that are mechanically flexible.

Depending on the periodic pattern of the metal grids, the filters have either simple high-pass, band stop or a more complex transmission characteristics. The critical frequencies of the filters depend on the spatial periodicity of the metal grids and the inter-layer separation. The transmission characteristic of these filters show cut-off frequencies in the far-infrared region with very high attenuation (>35dB) and large fractional bandwidths.

The measured values are in good agreement with theoretical results. This work also proves the scaleable behavior of the earlier metallic layer-by-layer PBG fabricated at Iowa State in the microwave regime. The new fabrication technique makes the structure very light weight, compact and flexible. The filters maintain their optical characteristics after repeated bending, demonstrating mechanical robustness of the metallic PBG structure. Rapid cooling of the samples in liquid nitrogen also does not show any visible stress on the sample or its optical characteristics making them excellent candidates for space applications.

The success of this fabrication technique, its simplicity and very good performance has led to more research funding on this project for further exploration of MPBG structures as infrared filters in space-based applications.

II. LITERATURE REVIEW

II.1 Photonic Band Gap Structures

The idea of photonic band gaps was first proposed by Yablonovitch in 1987 [1]. The idea is analogous to the behavior of electrons in a crystal lattice. The electromagnetic waves propagating in a structure with a periodically modulated dielectric constant are organized in "photonic bands" which are separated by "gaps" where propagating states are forbidden.

Following the inception of this idea, various lattice geometries were studied to find a periodic structure that would exhibit a photonic band gap in all the directions. After several unsuccessful attempts in finding the right lattice geometry using "trial-and-error" techniques, Ho et al. [12] at Iowa State University were first to predict the existence of a complete band gap in a periodic dielectric structure arranged in diamond lattice geometry. Diamond lattice structures were calculated to have large gaps for refractive index ratio between the two dielectrics as low as two.

II.2 First 3D-PBG structure

With these findings, Yablonovitch et al. [13] fabricated the first three-dimensional photonic band gap structure. The structure was arranged in a periodic face-centered-cubic lattice, but with cylindrical air holes, giving it an over-all diamond lattice structure. The periodicity in the structure was achieved by drilling holes 120° apart and at 35° from the z-axis into a dielectric slab as shown in Fig. 1. This experimental structure exhibited a full 3-D photonic band gap. It had a forbidden gap from 13 to 16 GHz with 10 dB attenuation per unit cell.

However, the structure has proved difficult to fabricate at optical frequencies where feature sizes are less than one micron. Chemically assisted ion beam etching technology has been used to etch the holes [14]. It has been found difficult to maintain the linearity and hole size as the etching depth increases. This adversely affects the periodicity of the structure and hence the photonic band gap. The midgap optical reflectivity is found to be very sensitive to structural errors in the photonic crystal.

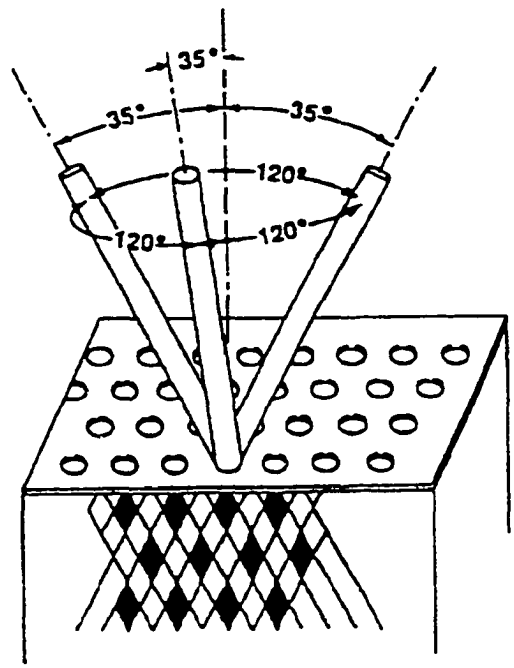

Figure 1: First purely three dimensional dielectric PBG structure fabricated by drilling holes at 35° to normal and 120° to each other [13].

II.3 Iowa State's layer-by-layer structure

After the initial verification of the existence of photonic band gap, there was an increased effort to find new structures that could be easily fabricated. Another structure that exhibited a complete band gap was suggested by Ho et al. [15] and fabricated by Ozbay et al. [16] from Iowa State. This new "layer-by-layer" structure was fabricated by stacking layers of equally spaced round or rectangular rods as shown in Fig. 2. The first layer-by-layer structure

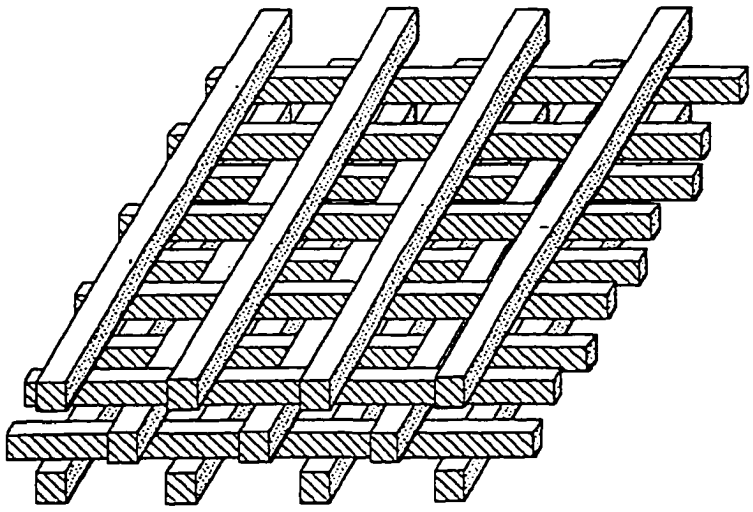

Figure 2: First layer-by-layer dielectric PBG structure fabricated at Iowa State [17]

was fabricated using alumina rods with dielectric constant $\varepsilon = 9.6$ glued together to form a face-centered-tetrahedral symmetry. This structure was found much easier to scale down in size [17]. Standard silicon micromachining techniques have been used to scale down the size of layer-by-layer PBG structure and make it operational up to 500 GHz at Iowa State University. Other laser prototyping methods have been used to fabricate this structure to about 2 THz [18].

II.4 Metallic PBG Structures

Fabrication of PBG structure has been mostly studied using frequency independent dielectric materials with positive dielectric constants where the possible problems related to absorption can be neglected. However, recent work on PBG structures using metals has shown good results for operating frequencies much lower than the plasma frequency of the metal. Although metals are quite lossy at optical frequencies, they act as nearly perfect reflectors at lower frequencies. The initial interest in metallic photonic band gap (MPBG) structures arose from the fact that they show higher attenuation with fewer layers as compared to their dielectric counterparts. These structures are much more compact, lighter weight and can be fabricated at a reduced cost as compared to dielectric structures.

The first MPBG structure with a complete 3-D band gap was reported by Yablonovitch et al. [19] in 1996. The MPBG structure had a geometry resembling covalently bonded diamond as shown in Fig. 3(a). Copper wire strips shown in Fig. 3(b) snap together to make diamond geometry. The transmission spectrum of this structure did show a forbidden gap similar to a purely dielectric structure centered about v_0, corresponding to the lattice constant of the structure. But this forbidden gap does not extend in all the directions. In addition to this forbidden gap, this structure shows a new 3-D bandgap that extends from zero to a cutoff frequency of ~(1/2) v_0. This high pass spectrum of the structure can be observed in all the directions and is called the metallicity gap. The structure shown in Fig. 3 has a high pass cutoff frequency of 6.5GHz. The effect of introducing defects into the structure was also studied in detail. However, because of the complex geometry of the structure it has been difficult to scale down its size.

Another layer-by-layer structure for metallic photonic crystal fabricated at Iowa State University by McCalmont et al. [20] has shown very good results. The structure is built by stacking three layers of square metallic grids aligned to each other and separated by a

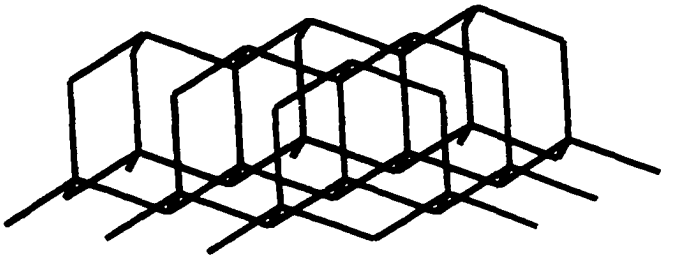

(a)

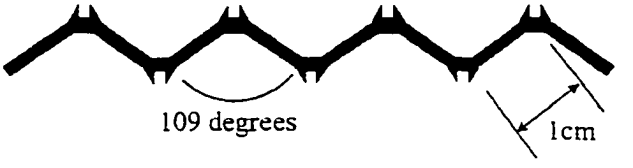

(b)

Figure 3: (a) First three dimensional metallic PBG structure with a diamond lattice symmetry formed by snapping (b) metal wire strip with neighboring arms at 109° and arm length 1cm [19].

dielectric medium as shown in Fig. 4. The transmission characteristic of the structure exhibits a metallicity gap with as few as three metal layers in the stacking direction. The location of the band edge is a function of lattice constant, width of the metal wire grid, and the refractive index of the dielectric material. This structure was fabricated on a duroid ($\varepsilon_r = 1.5$) printed circuit board with copper laminations on both sides. One side of the copper cladding was patterned with the grid pattern using standard photolithography techniques and the backside copper was completely removed. The structures were fabricated to operate in 75-110 GHz frequency range.

A change in periodicity of the center grid creates a defect mode in the band gap region, effectively forming a bandpass characteristic. The size of the defect determined the location of the defect mode frequency in the band gap. The response of the structure is virtually unchanged over a wide range of incident angles, but it is not a fully three-dimensional structure.

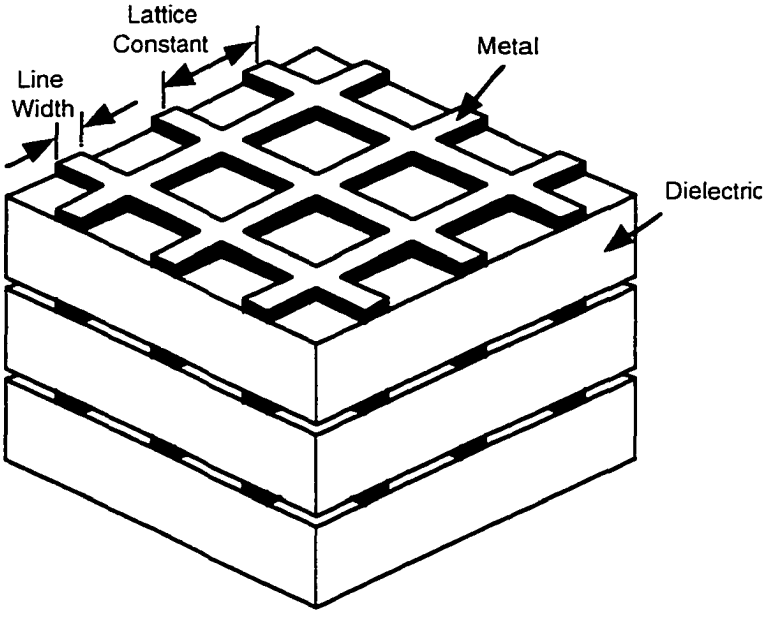

Figure 4: First layer-by-layer metallic PBG structure fabricated at Iowa State [20]

Both the transmission and reflection characteristic of the defect peak were measured. The reflected peak was much sharper than the transmission peak with a maximum measured quality factor of 461 in the reflection measurements. This structure has been fabricated in the far-infrared region [21] with good results. The details of the far-infrared structure and its characteristics are a part of this thesis.

McIntosh et al. [22] studied a lattice geometry where metallic atoms were located on

a three-dimensional (100) oriented face-centered-cubic (FCC) lattice, and the sites were isolated from each other. Initially they studied the characteristics of this structure in the microwave region and then extended this concept to the infrared. The metallic FCC structure was embedded in a polymer and supported on a silicon substrate. This group fabricated two different sets of arrays.

The first set had its lattice sites occupied with square metal patches while the other set of arrays had circular patches. The lattice constants of different structures ranged from 2 to 4 μm. These structures show band gap behavior that is very similar to the dielectric PBGs. The circular patch structures showed frequency gaps at 3650 cm^{-1} with a maximum attenuation of 15 dB and a gap to midgap ratio of 0.21. The circular patch had diameter, D = 1.06 μm and center-to-center spacing, S = 1.7 μm. The FCC structures with square patches at the lattice points had a maximum attenuation of 21 dB with center frequency of 1450 cm^{-1} and a gap-to-midgap ratio of 0.83. The metal patches were 2 μm wide and the center-to-center spacing was 3.18 μm.

These structures definitely have very high operating frequencies, but their attenuation is relatively low, and all of the measured values have been compensated by subtracting the silicon transmission spectrum. For this structure to be used as a filter, the silicon substrate would always be a problem. The new scheme developed and explained in later chapters would solve this problem by removing the substrate completely. In addition, the band gaps in the samples of McIntosh et al. are also compensated by subtracting polyimide absorption. Separating the effects of the photonic band gap structure from the material absorption is problematic, and this overlap would preclude use of the structure from most applications.

II.5 Frequency Selective Surfaces

The layer-by-layer MPBG structures described earlier are related to frequency selective surfaces (FSSs). Frequency selective surfaces are two-dimensional arrays of metallic aperture elements or patches that have frequency-filtering properties. They have been studied in great detail because of their application as filters, bandpass radomes, polarizers and mirrors in microwave and far-infrared region. Different aperture and patch element geometries (e.g. square patch, circular patch, cross dipole, Jerusalem cross, square loop, circular loop, square aperture etc.) have been studied [8].

Most of the experimental work reported on FSS has been for single layer structures, and no results have been reported for true three dimensional structure. Single-layer free-standing copper grid structures 12 μm thick have been reported with frequencies near the 2 THz, but the structure shows an attenuation of only 18 dB [23].

Metallic PBG structures have much higher attenuation in the band gap region as compared to single layer FSSs. The metallic PBG is a three-dimensional structure which provides the unique advantage of creating a defect mode in the stopband region by disturbing the periodicity of the structure. Defect peak frequencies with very high quality factors have been reported. The layer-by-layer interconnected metallic structure discussed earlier show a quality factor, Q of 461. Quality factor is defined as the ratio of peak frequency to the 13 dB (half power) bandwidth of the peak. Also, the frequency of an MPBG defect peak is adjustable and is a function of the size of the defect introduced.

III. DESIGN AND FABRICATION

This chapter describes the design and fabrication of mechanically flexible MPBG structures with critical wavelengths in the far infrared. The basic MPBG structure consists of three layers of metallic mesh aligned to each other and separated by a dielectric medium, as shown in Fig. 4. This type of MPBG structure operating at millimeter-wave frequencies has been previously demonstrated [19]. The lower frequency structures were built using printed-circuit board technology and were studied for square metallic grid patterns only. The present work uses semiconductor process techniques to scale the metallic PBG structure to infrared region and studies various other lattice geometries and their characteristics. The transmission spectra of the different lattice geometries is initially calculated and the critical dimensions for mask generation are derived theoretically before fabrication.

III.1 Calculations

Prior to fabrication, the expected transmission spectrum for a particular structure is calculated using the transfer matrix method (TMM) originally introduced by Pendry and MacKinnon [24]. All the theoretical results presented in this work have been performed by M. M. Sigalas in the Department of Physics and Astronomy at Iowa State University. In the TMM technique the total volume of the unit cell PBG is divided into small cells, and the fields associated with each cell are coupled to neighboring cells. The final transfer matrix relates the incident wave on the PBG from one side to the outgoing wave on the other side. The TMM can be used to calculate the band structure of an infinite periodic system. However, for these studies, the TMM is used to determine the electromagnetic transmission and reflection coefficients as functions of frequency for waves incident on a PBG of finite thickness. The transfer matrix method has previously been applied in studies of defects in 2D PBG structures,

of PBG materials with complex and frequency dependent dielectric constants [7], of 3D layer-by-layer PBG structure, [17] and of 2D metallic structure [25]. In all those previous investigations, the theoretical results matched very well with experimental measurements.

The calculations for all the metallic structures have assumed a frequency-dependent dielectric constant for metal [7]

$$\varepsilon(\upsilon) = 1 - \frac{\upsilon_p^2}{\upsilon(\upsilon - i\gamma)} \quad . \tag{9}$$

where υ_p = 3600 THz and γ= 340 THz are the plasma frequency and the absorption value. The above equation can also be written as:

$$\varepsilon(\upsilon) = \varepsilon'(\upsilon) - i\varepsilon''(\upsilon) \tag{11}$$

where $$\varepsilon''(\upsilon) = \frac{4\pi\sigma}{\omega} \tag{12}$$

and $$\omega = 2\pi\upsilon. \tag{13}$$

From the above equation, it can be shown that the conductivity is

$$\sigma = \frac{\upsilon_p^2 \gamma}{2(\gamma^2 + \upsilon^2)}. \tag{14}$$

Similarly, the skin depth is

$$\delta = c\frac{(\mu\upsilon\sigma)^{-1/2}}{2\pi}. \qquad (15)$$

where c is the velocity of light and μ is the magnetic permeability. For frequencies smaller than 100 THz, σ can be practically assumed to be independent of frequency and equal to 0.22×10^5 $(\Omega\ \text{cm})^{-1}$. The value of conductivity is chosen to be close to the measured conductivity of Ti. For υ = 100 THz and 10 THz, the skin depth would be 0.035 μm and 0.11 μm, respectively.

III.2 Fabrication of MPBG structure

The metallic photonic bandgap structures were fabricated in a layer-by-layer fashion using alternating layers of polyimide for the dielectric and aluminum metal for the grids. The MPBG structures can cover any size area, but we typically used patterns covering an area of 2 × 2 cm. The layers for all the structures were fabricate on 2 inch GaAs substrate. A standard spin-on fluorinated polyiamic acid polyimide (DuPont Pyralin® SP series PI-1111) having a dielectric constant $\varepsilon_r = 2.8$ was used for the dielectric. Its chemical structure is designed to impart good mechanical and electrical properties. It has an adhesion promoter chemistry incorporated directly into the formulation, eliminating the need for a priming cycle before coating.

The spin-on polyimide is first softbaked at 130°C for 30 mins which removes most of the solvent and produces partial imidization of the polyamic acid. After softbake the layer is cured at 350°C for another half hour to complete the imidization and consolidation of the film. Care is taken to introduce the sample into the furnace at 200°C, and then the temperature is slowly ramped to 350°C to minimize substrate deformation. The sample is cured for 30 mins at 350°C, and then the furnace is cooled down to 200°C before removing the sample. The samples

for which the desired thickness of separation layers is more than 11 μm. multiple coats are required to make one thick layer. The process is similar to the single coat processing. First polyimide is spun-on and softbaked. Then another polyimide coat is spun on the top of the first layer, followed by another softbake. Finally the sample is cured at 350°C to complete the process. The transmission characteristics of cured PI-1111 is good in the 2 to 8 THz frequency region as shown in Fig. 5 for a 45 μm thick layer. There are two strong absorption bands centered around 10 and 16 THz, and these frequency bands must be avoided in building the MPBG structure. The dimensions of MPBG structure are chosen so that the critical frequencies

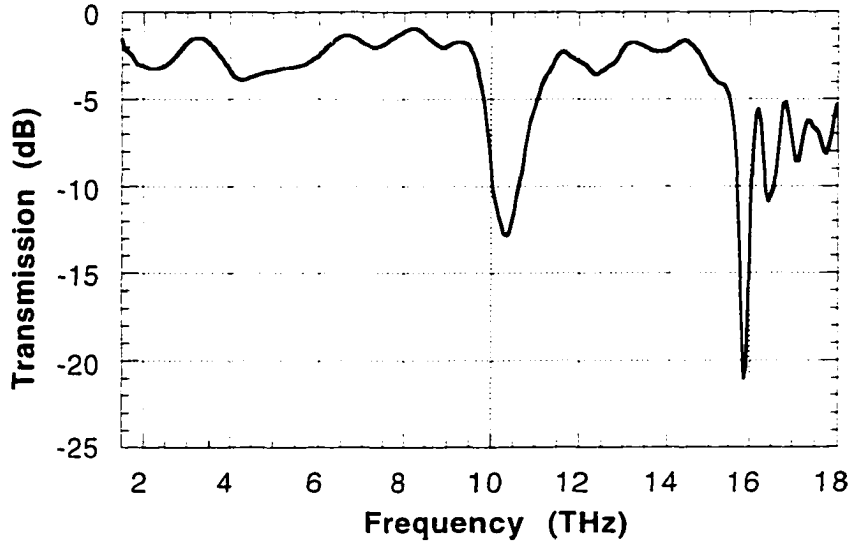

Figure 5: Transmission vs frequency spectrum of a 45μm thick polyimide film.

are safely below the absorption bands.

The aluminum metal grid pattern is formed on the polyimide using standard lift-off techniques. First, AZ-5209E photoresist is spun onto the surface of polyimide at 3000 rpm and is baked at 90°C for 30 minutes. It is exposed to UV light with the negative of the grid pattern.

The exposed photoresist is hardened in a chlorobenzene soak of 10 minutes, after which the pattern is developed. Then, a 2000 Å thick aluminum layer is deposited on the sample surface using e-beam evaporation. The deposition rate for aluminum is maintained within 7 to 10 Å/sec. The thickness of the photoresist is about 1μm which is good enough for the lift off of 2000 Å metal. The sample is now treated with acetone in an ultrasonic bath to remove unwanted aluminum by dissolving the photoresist underneath. The standard lift-off process is explained in more detail in appendix II.

The polyimide and metal deposition is repeated to make the 3-layer MPBG structure. After completing the three metal layers, another thin 5 μm coating of polyimide is spun on and cured. The sample is now treated in a solution of citric acid and hydrogen peroxide (4:1) to etch away the GaAs substrate, a process that typically requires 30 hrs. At the end of the GaAs etching step a flexible sheet of polyimide is left with the metallic PBG embedded in it as shown in Fig. 6. The complete MPBG structure is encapsulated by 5 μm thick coating of polyimide on the top and bottom.

Several sets of samples with different lattice geometries were fabricated to systematically study the transmission and reflection characteristics. All the samples have total polyimide thickness of 9 μm to 60 μm depending on the particular structure.

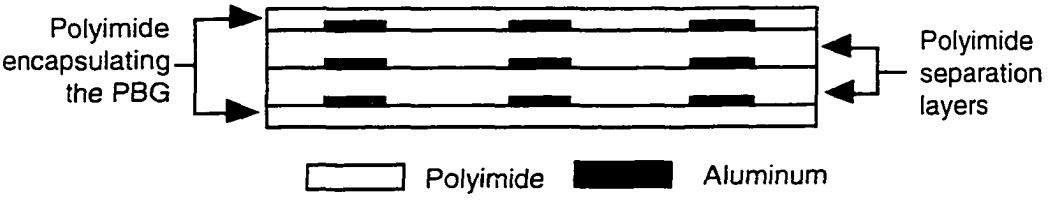

Figure 6: Cross section of the flexible metallic PBG structure encapsulated in polyimide.

IV. MEASUREMENTS

The transmission characteristics of the MPBG structures were measured using a Fourier transform infrared (FTIR) spectrometer (Nicolet model Magna IR 760), which can measure over a range of 1.5 THz to 330 THz. The minimum relative response of the system is 35dB. The basics of an FTIR are explained in Appendix III. All the measurements were done using an unpolarized beam. Most of the transmission measurements were done with incoming beam at normal incidence. All the reflection measurements were at an 11° angle of incidence. Transmitted and reflected power measurements are presented on a logarithmic scale.

For all the measurements, the spectral resolution was 0.06 THz. In the typical measurement, the results were obtained by averaging over 200 scans. The sample chamber of FTIR is nitrogen purged during measurements. Nitrogen purging helps to remove water vapor and carbon dioxide, which introduce absorption bands in the measured spectrum. The noise level in an FTIR falls as the square root of the number of scans. Measurements averaged over 200 scans reduce noise level significantly. The transmission and reflection spectra of the structures are discussed in the following sections.

IV.1 High-pass filters

The first family of metallic PBG structures that were studied had high-pass transmission characteristics. The structures had three layers of square metal grids aligned to each other. The metallic PBG has the same geometry used by McCalmont et al. [20] at lower frequencies. The top view of the metal grid structure is shown in Fig. 7. Mask sets with different lattice constants and line widths were designed and fabricated in-house. The different mask set details are listed in Table 1.

Several samples were fabricated using these three mask sets. The transmission and reflection characteristics of these structures were measured and compared with the theoretical calculations. The characteristics of these MPBG structures were also studied as a function of lattice constant, number of metal layers and thickness of dielectric medium separating the adjacent layers.

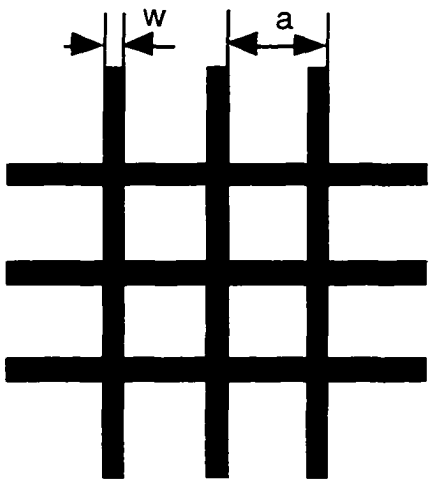

Figure 7: Pattern on the mask sets is a square grid with lattice constant, a and line width, w.

Table 1: Sample sets for square metal grid with different lattice constants and line widths

Mask Set	**Lattice Constant, a (μm)**	**Line Width, w (μm)**
Set A	32	5
Set B	16	2.5
Set C	11	1.5

The measured and calculated transmission characteristics of a three-metal-layer structure fabricated using mask set B with lattice constant of 16 μm and inter-layer separation of 11 μm are shown in Fig. 8. The structure shows the expected high-pass behavior with a cutoff at about 6.5 THz. The measured transmission curve shows an attenuation of more than 35 dB in the stopband region, while in the transmitting region the attenuation is about 2 dB. The measurements agree well with predicted results, although the measured transmission in the pass-band is somewhat lower than expected.

All the results have a mismatch of about 18% between measured and calculated spectrum for all the interconnected structures discussed here. This is probably due to the poor convergence of the TMM calculations. Each unit cell has been divided into $N \times N \times N$ cells, where $N = 20$. The unit grid size for calculation within the unit cells would be $0.8 \times 0.8 \times 0.8$ μm. Using this grid dimension, as listed in Table 2, the structure defined in the

Table 2: Mismatch between the measured and calculated structures.

Feature	**Fabricated structure**	**Calculated structure**
Line width	2.5μm	3.2μm
Inter-layer separation	11μm	11.2μm
Metal layer thickness	0.2μm	0.8μm

calculations has dimensions that are different for the measured structure. A higher value of N would be needed for better convergence.

From Table 2, we can see that the line-width in the calculation is 0.7 μm more than the fabricated structure, the inter-layer separation is off by 0.2 μm and the thickness of the

metal is 0.8 μm as compared to 0.2 μm in the fabricated structure. These mismatches in the calculated and measured geometry would significantly affect the characteristics of the structure.

Another major cause of mismatch would be the absorption due to polyimide. In the calculations the dielectric is assumed to have no absorption. This results in very high quality factors and excellent transmission and reflection characteristics for theoretical but which are not seen in our measurements.

Figure 8 also shows the reflection characteristic of the MPBG structure at 11° angle-of-incidence. As expected, the reflection in the stopband region is very high with an attenuation of less than 1 dB in the stopband region. The reflection drops down to 16 dB outside the gap near 6.5 THz region. The presence of a higher-order bandgap is very prominent in the reflection spectrum where an increasing trend in the reflection characteristic above 6.5 THz can be noticed.

The next set of measurements show the relationship between cutoff frequency of the high-pass structure and the lattice constant of the square metallic grid. The two measured transmission spectra of Fig. 9 show two three-layer structures fabricated using mask sets A (a = 32 μm) and B (a = 16 μm) with polyimide spacers of 17 μm and 11 μm respectively. Figure 9 shows that reducing the lattice constant of the metal grid increases the cutoff frequency of the high-pass filter. The 32 μm structure with 5 μm line width shows a cutoff at about 3.0 THz while the 16 μm structure with 2.5 μm line width shows a higher cutoff frequency near 6.5 THz. The attenuation in the transmitting region of the MPBG with 32 μm lattice constant is about 4 dB as compared to only 2 dB in the 16 μm structure. This is a direct result of the fact that total polyimide thickness in the 32 μm MPBG is about 44 μm and has more absorption as compared to thinner 32 μm polyimide in the 16 μm MPBG structure.

The effect of the number of layers in the MPBG structure is shown in Fig. 10, which shows transmission spectra for 1, 2, 3 and 4 layer MPBGs. Note that the 1-layer MPBG structure is identical to an FSS. The grid with lattice constant of 16 μm is used for

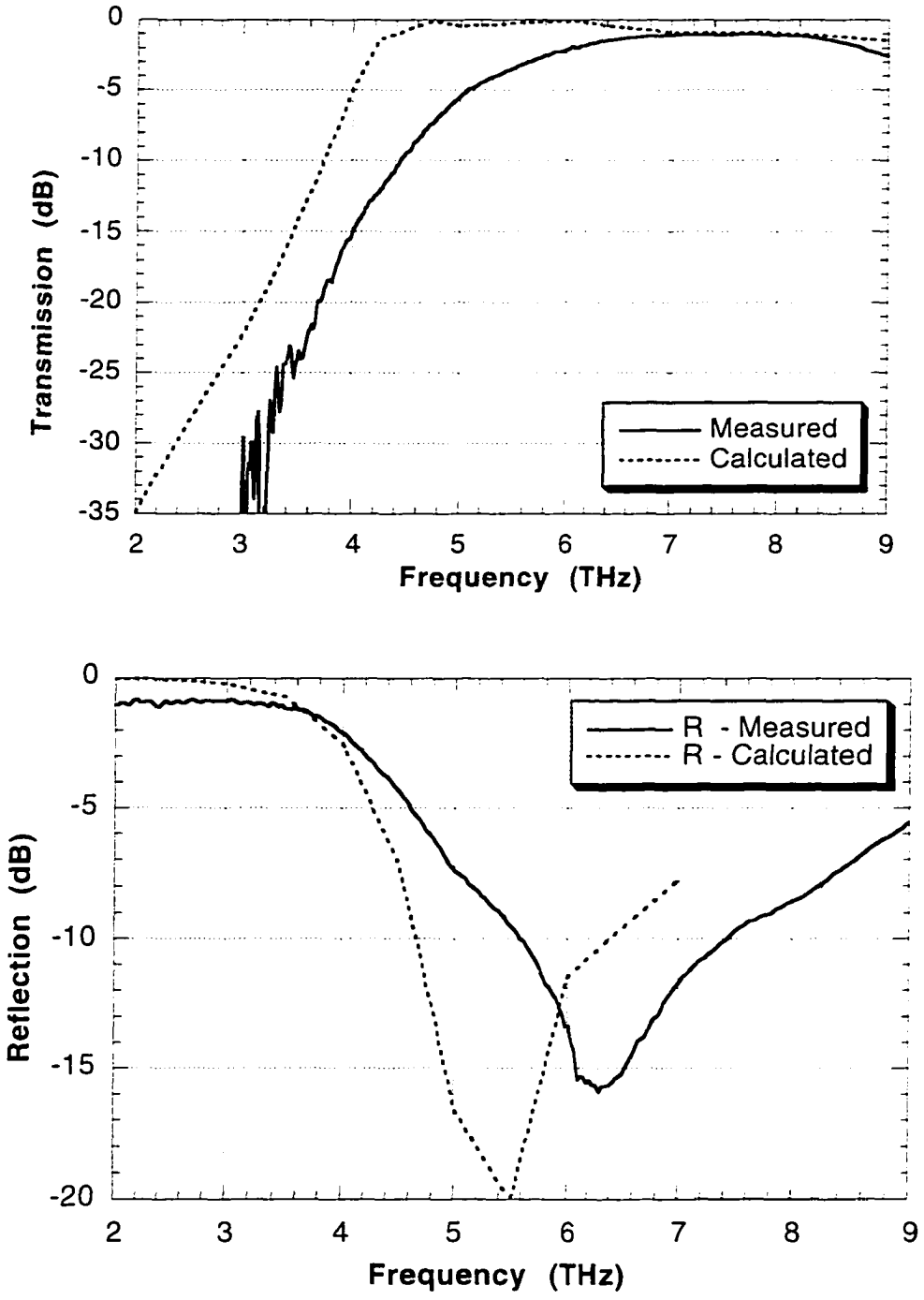

Figure 8: Transmission and reflection measurements on the sample set with a = 16 μm, w = 2.5 μm (3.2 μm for calculations) and inter-layer separation 11 μm.

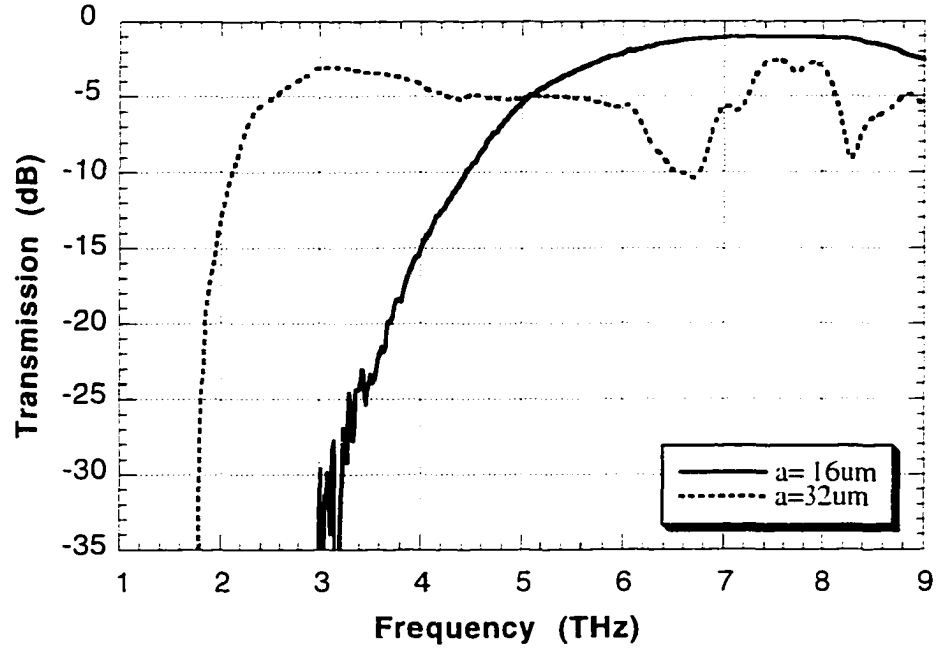

Figure 9: Comparison between the transmission measurements of sample set A and B. For set A and B the inter-layer separations are 17 μm and 11 μm respectively.

these samples. The attenuation in the stopband region of the three-layer MPBG with 35 dB is significantly better than the FSS with 12 dB. The MPBG structure also has a much higher rate of attenuation (i.e. slope of transmission edge) from pass-band to the stopband region at 15 dB/THz as compared to 2.2 dB/THz for the single layer FSS. It can also be concluded from Fig. 10 that the attenuation per layer is about 12 dB. The four-layer structure should have a higher drop in the band-gap region, but due to the limitations of the measuring instrument, its true value cannot be measured. The drop in transmission in the pass-band region of the four layer structure shows a significant attenuation of about 4 dB, which may be due to absorption in the polyimide. We can also see the interference fringes created because of polyimide thickness.

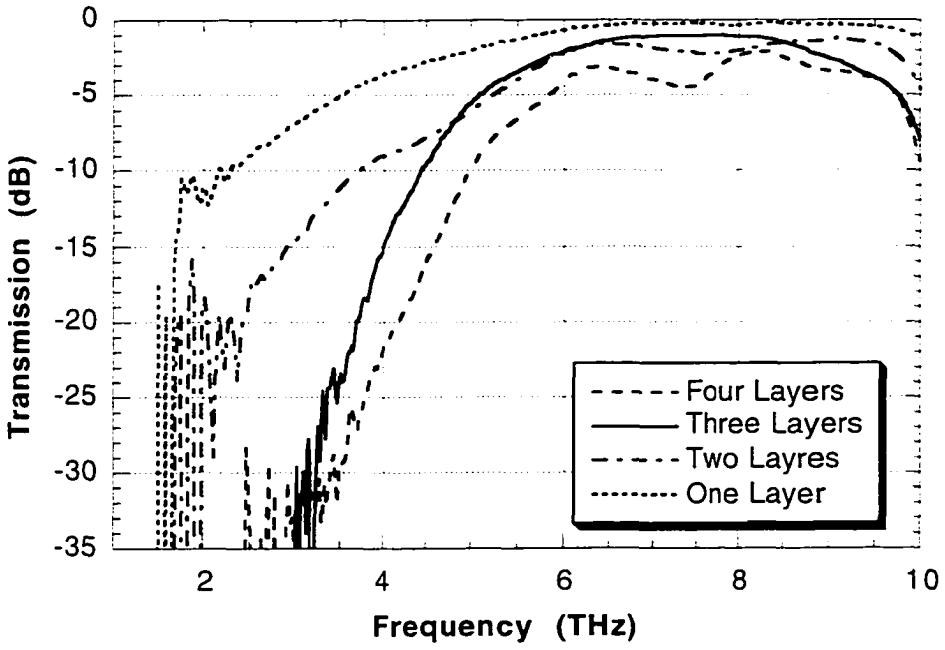

Figure 10: Attenuation in the band gap region as a function of number of layers. The dimensions are lattice constant, a = 16 μm, line width, w = 2.5 μm and inter-layer separation = 11 μm. Attenuation per layer in the bandgap region is about 12 dB.

The cutoff frequencies of the structures are also found to be a somewhat dependent on the polyimide spacer thickness. The dependence is not strong, but the effect can be used for fine adjustment of the cut-off frequency. This feature is particularly useful when the mask set is already designed for the filter to operate at a certain frequency and minor frequency adjustments are required. Figure 11 shows the measured values for two-layer metallic structures fabricated using mask set A with lattice constant, a = 32 μm. A 35 μm polyimide spacer results in a cutoff frequency of 1.9 THz. Reducing the interlayer separation to 17 μm increases the cutoff to a value of 3 THz for the same grid size. Further reducing the polyimide spacer to 11 μm moves the cutoff to 3.4 THz. However, it is clear from the measurements that,

as the interlayer separation is reduced, the attenuation in the bandgap also reduces. For a separation of only 11 μm, the two-layer structure almost behaves like a single layer FSS with attenuation of only 12 dB in the bandgap region. Another feature to be noticed in the 35 μm sample is the presence of a higher order bandgap centered near 2.5 THz which is not visible in

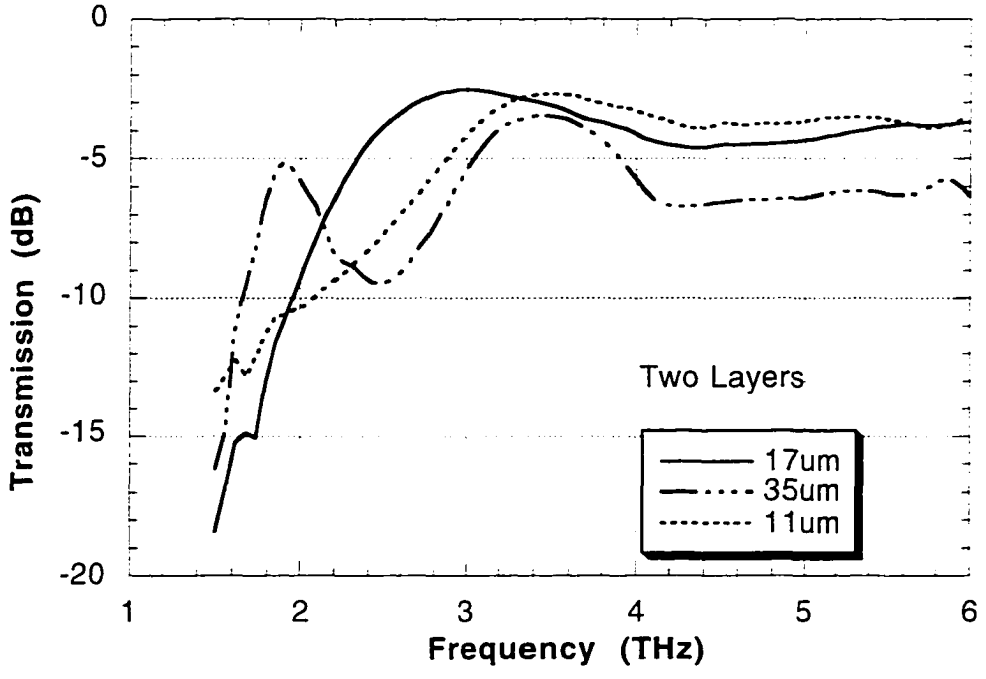

Figure 11: Change in cutoff frequency as a function of inter-layer separation. Reducing the inter-layer separation increases the cutoff frequency. Each layer has a = 32 μm and w = 5 μm.

the samples with smaller separations. This effect can be seen in the figure for the spectrum having 35 μm inter-layer separation.

The filter characteristic changes very little as the incidence angle is varied from 90° to 40°. The cut-off frequency is nearly independent of incidence angle in that range, and the transmission in the bandgap region changes from 35 dB at normal incidence to 30 dB at 40°.

IV.2. Localized defect modes

The effects of introducing a defect in the structure by disturbing its periodicity are discussed here. The defect is introduced in the middle layer of the three-layer MPBG structure. The defect layer has a portion of the metal grid removed from every other intersection, as shown in Fig. 12.

The defect structures were fabricated for mask set B which has a lattice constant, a = 16 μm and line width, w = 2.5 μm. The radius of metal removed from every other cross section, r_d had values of 4.75 μm, 6.75 μm and 10.75 μm. The inter-layer separation between the adjacent metal grids was maintained at 11 μm. As usual, these samples had a top and bottom 5 μm polyimide layer encapsulating the structure.

The transmission and reflection measurements are performed on different sets of defect structures. Figure 13 confirms the presence of a defect mode created by disturbing the periodicity of the structure. The simulated transmission response is in fairly good agreement with the measured data. The defect radius introduced in the measured structure was 4.75 μm, which introduces a defect peak near 3 THz. The peak transmission is about 8.5 dB at the peak and has a quality factor Q of 10. The quality factor, Q is defined as

$$Q = \frac{f_p}{BW} \tag{16}$$

where f_p is the frequency at which the intensity is maximum and bandwidth, BW is the frequency range around f_p outside which the intensity falls to 3 dB below the peak intensity. The calculated defect frequencies have much higher peak intensity and quality factor as compared to the measurements. This may be due to the fact absorption in the polyimide is not accounted for in the theoretical calculations and the line width used for calculation purpose is

3.2 μm as compared to 2.5 μm in the actual structure.

The transmission characteristics of the MPBG structure with defects have also been studied as a function of change in defect radius. Figure 14 shows the transmission characteristic of the structures with different defect radii. It can be seen that as r_d increases from 4.75 μm to 10.75 μm, the defect peak frequency increases from 3 THz to 4 THz and moves

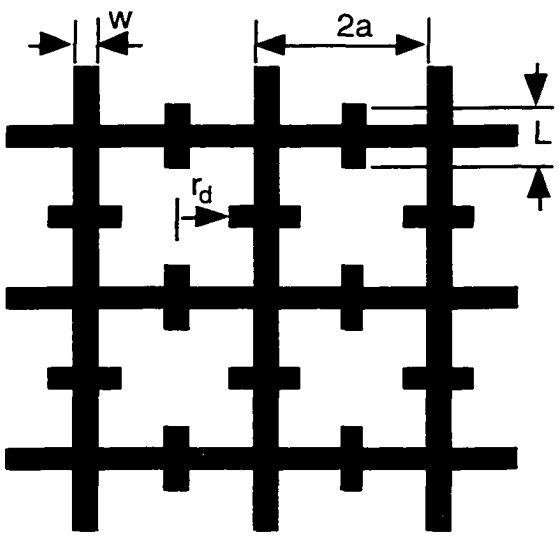

Figure 12: Defect layer introduced in the middle layer of the metallic PBG structure. L is the length of the cross-arm, r_d is the radius of metal removed from every other intersection.

nearer the band edge. This is in good agreement with theoretical calculations which show a similar trend. These measurements also show that as the defect radius increases, the peak intensity of the defect modes moves to higher frequencies but the quality factor of the peak reduces. For r_d = 10.75 μm, the attenuation at the defect peak is only 4.5 dB but the peak broadens and the Q value is very low. Again, the absorption due to polyimide reduces the intensity of defect peaks.

The reflection measurements of the these defect peaks are shown in Fig. 15. All the reflection measurements were taken at an 11° angle-of-incidence. The respective defect peaks in the transmission spectrum show a dip in reflection at respective frequencies. But in these cases also, the reflection dip as well as the Q values are very low which may be due to polyimide absorption. For the structure with r_d = 4.75 μm, the reflection in the bandgap region is 95% and near the defect peak frequency of 3 THz, the reflection dips down to only about 60% which is even less than 1 dB.

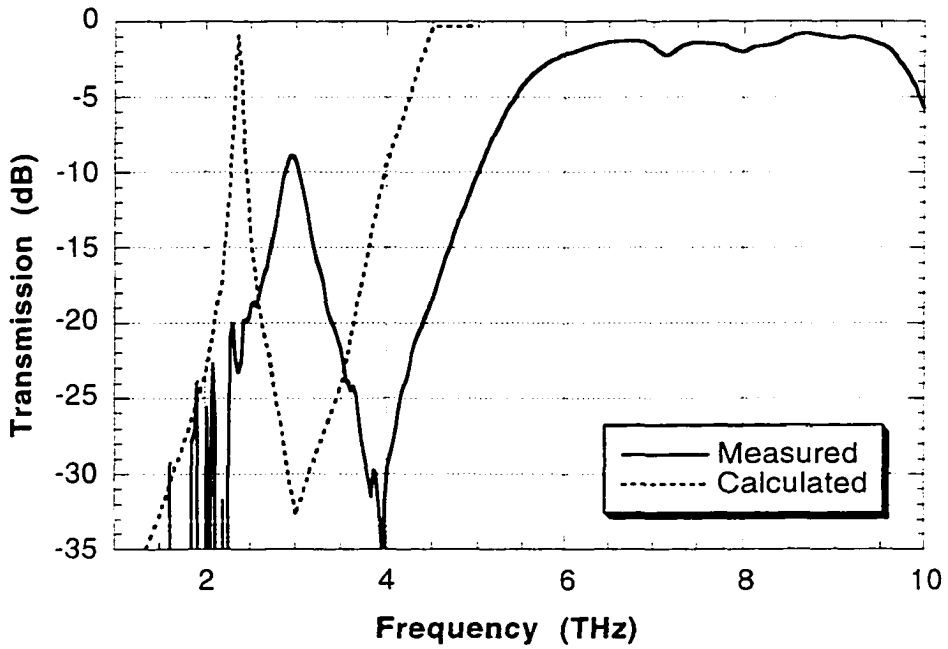

Figure 13: Measured and calculated defect peaks in the bandgap region. The structure has defect radius, r_d = 4.75 μm with a = 32 μm, w = 2.5 μm (3.2 μm in calculation) and inter-layer separation = 11 μm (11.2 μm in calculation). The measured defect peak frequency occurs near 2.9 THz.

The transmission characteristics of the defect structures were also studied as a function of inter-layer separation. For the same defect radii, a new set of structures was fabricated with inter-layer separation of 20 μm as compared to the earlier value of 11 μm. The first thing to notice is that the band-edge shifts down in frequency and the higher-order band gap becomes very prominent, as was observed in the earlier periodic square grid results of Fig. 11. In the results shown earlier in the chapter, for a structure with lattice constant of 32 μm with inter-layer separation 35 μm, the higher-order bandgap is very prominent. It is clear from

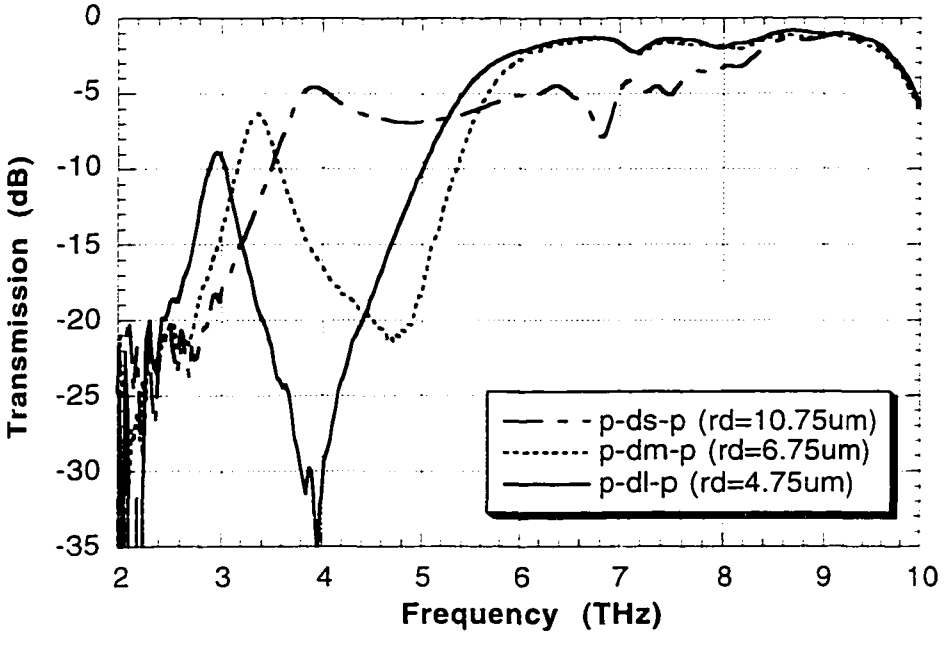

Figure 14: Defect peak as a function of the defect radius, r_d. Increasing defect radius increases the defect frequency but the Q value reduces. Here, a = 16 μm, w = 2.5 μm and inter-layer separation = 11 μm.

the measurements that the edge of the bandgap and the defect peak frequency are reduced by increasing the inter-layer separation as shown in Fig. 16. The band-edge shifts from 6.5 THz to near 4 THz as can be seen from the transmission spectrum. For the 6.75 μm defect radius with lattice constant of 16 μm, the defect peak moves down to 2.5 THz from 3.4 THz as the

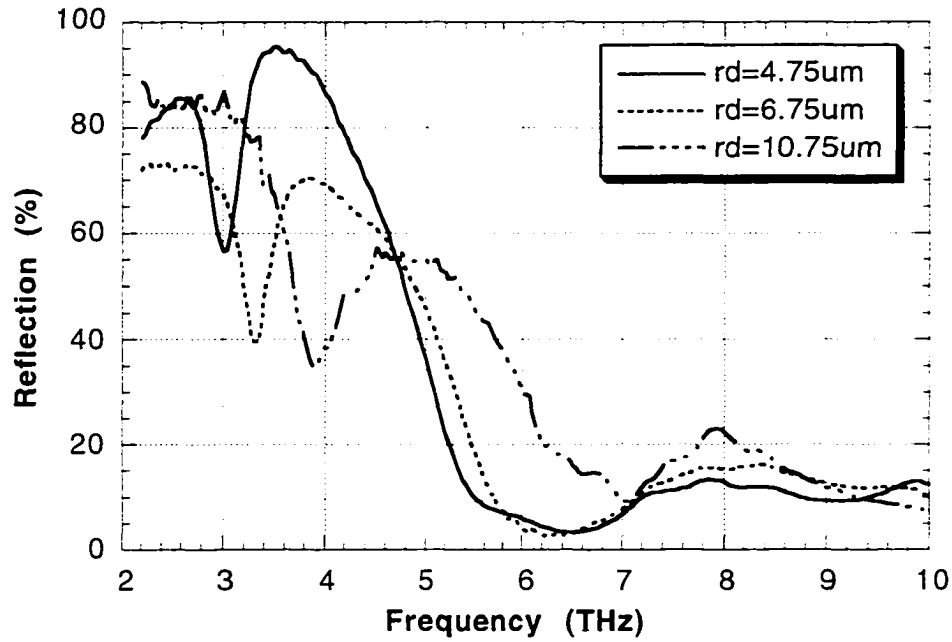

Figure 15: Reflection measurements on samples with different defect radii. Here, a = 16 μm, w = 2.5 μm and inter-layer separation = 11 μm.

separation between the layers increases from 11 μm to 20 μm. Reflection measurements show similar behavior as reported in the previous results. The strength of the defect peak is much lower in the reflection measurements.

The next set of measurements shows the effect of increasing the number of defect layers on the transmission characteristic of the MPBG structure. A sample was fabricated with

two defect layers between the top and bottom layers of periodic square metallic grids. The structure is fabricated for r_d = 10.75 μm. The transmission measurements of Fig. 17 show that by adding one more defect layer, the defect peak moves to a lower frequency of 2.2 THz from 2.9 THz. The defect peak has a higher attenuation, but its Q value has improved. The band edge of the structure also moved to a lower frequency of about 5.5 THz. The higher order bandgap near 7 THz shows a much higher attenuation of about 17 dB in the bandgap region. It can be concluded that increasing the number of defect layers improves the quality factor of the

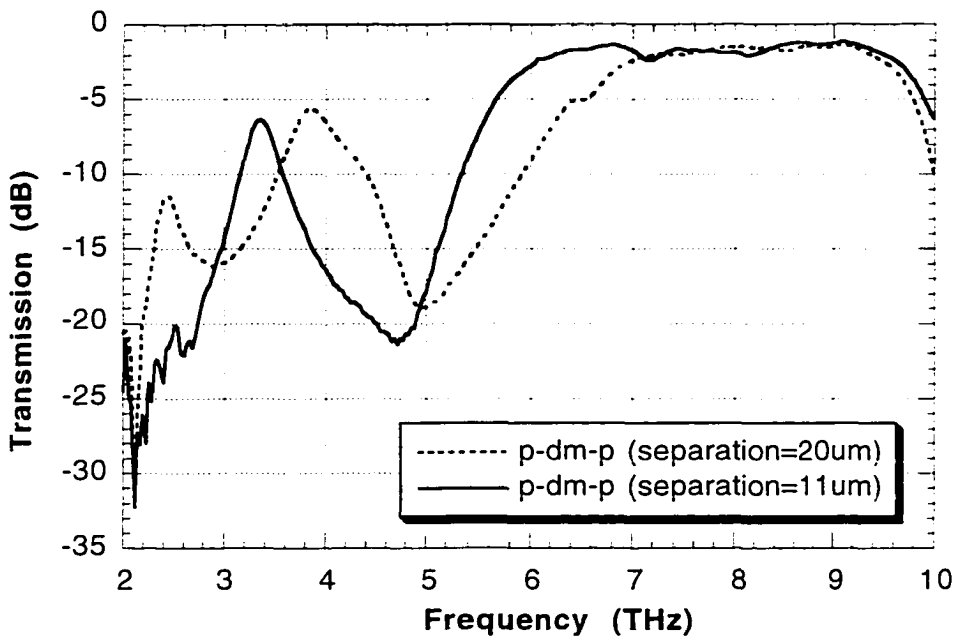

Figure 16: Change in defect peak as a function of inter-layer separation. Increasing inter-layer separation reduces the defect peak frequency. Here, r_d = 6.75 μm, a = 16 μm and w = 2.5 μm.

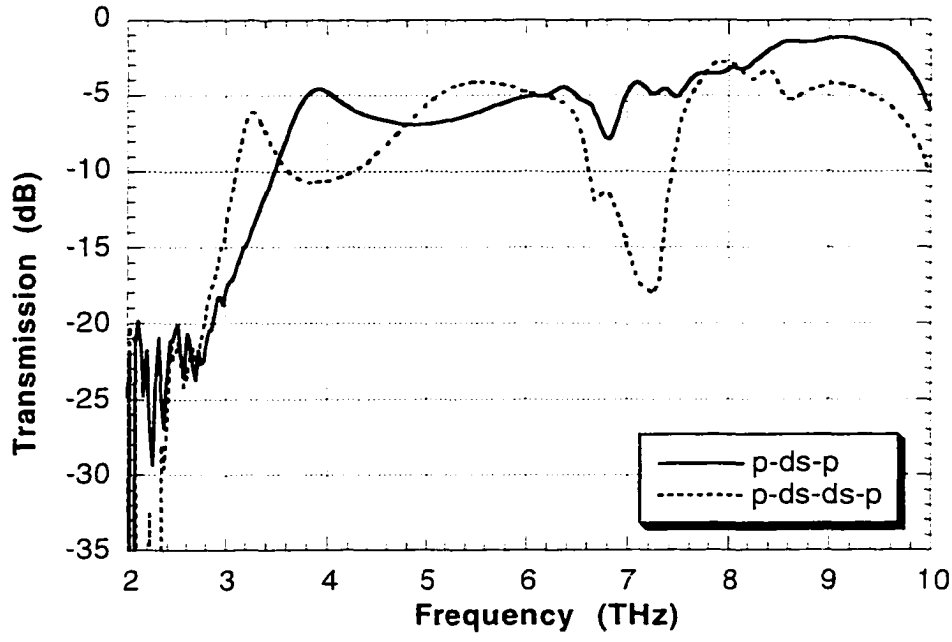

Figure 17: Change in defect peak as a function of number of defect layers. Here, r_d = 10.75 μm, a = 16 μm, w = 2.5 μm and inter-layer separation = 11 μm.

defect peak and moves it to a lower frequency. The higher order bandgap near 7 THz is a feature due to the defect layer. This will be more clear in the next section when bandreject filters are discussed in detail.

VII. Band-reject Filter

This section discusses the filter characteristic when the defect layer pattern is used for all the three layers of MPBG structure. We can also describe it as a periodic square metallic grid which has a metal bar of length L introduced normal to each arm of the square. Here, L is defined as $L = 2(a - r_d)$. This structure has a lattice periodicity of 32 μm and line width of 2.5

μm. The measurements show that by changing the pattern of the metal grid to include a periodic defect in all the layers, a rejection band can be introduced into the pass band of the original structure. The metal grid pattern used to effect this change is the same as shown in Fig. 12. Using the modified grid pattern, a three-layer MPBG structure with 11 μm inter-layer separation is fabricated. The measured and calculated transmission characteristic of the structure with cross-arm length, L = 22.5 μm are shown in Fig. 18.

The measurement results show a similar low frequency cut-off near 2.5 THz as shown in the earlier square grid structure with 32 μm lattice constant (see Fig. 9). In addition

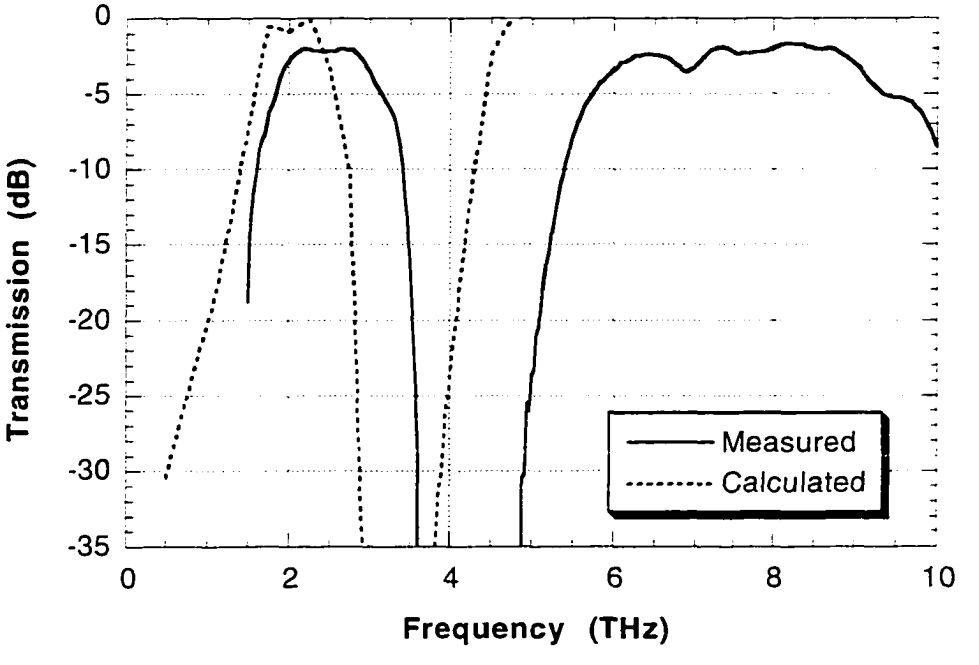

Figure 18: Measured vs calculated transmission spectrum for the band-reject filter with cross-arm length, L = 22.5 μm. Here, a = 16 μm, w = 2.5 μm (3.2 μm in calculations) and inter-layer separation = 11 μm (11.2 μm in calculations).

to this low cutoff frequency, there is a higher-order rejection band centered around 4 THz. The higher edge of this bandgap is near the cut-off frequency of the 16 μm square grid structure i.e. 6.5 THz. The band is deep, with rejection of more than 35 dB, and fairly wide, with a fractional band width of about 46%. The discrepancy between the measured and the calculated spectrum is approximately 18%. Again, this is due to the differences in the measured and calculated grid dimensions and absorption due to polyimide which are not included in simulations. The reflection spectrum of the structure in Fig. 19 shows an attenuation of about 2 dB in the higher order bandgap.

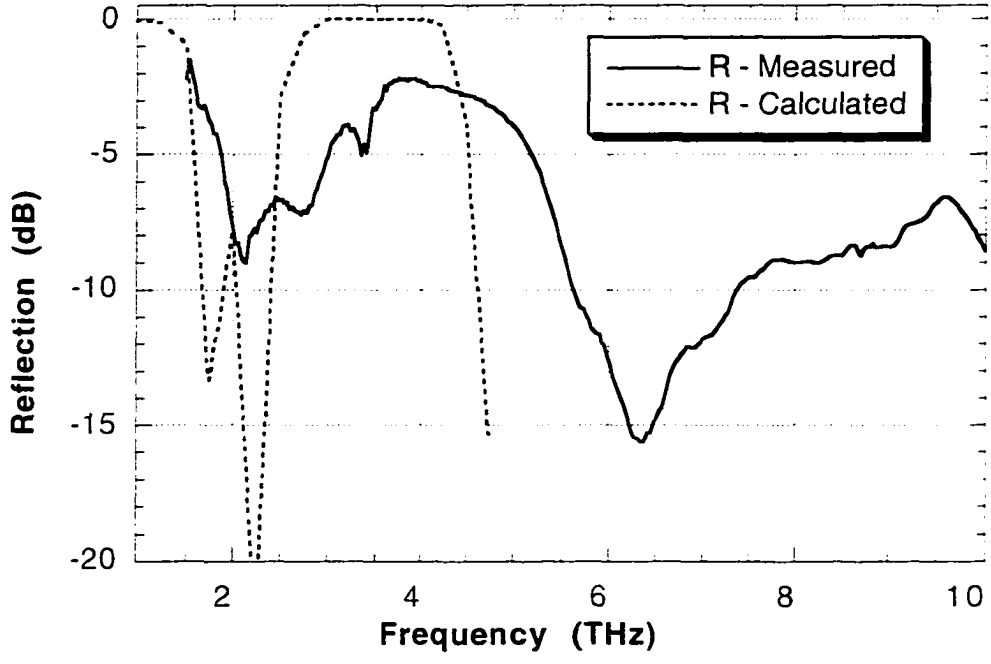

Figure 19: Reflection spectrum of the band-reject filter. Here, L = 22.5 μm, a = 16 μm, w = 2.5 μm (3.2 μm in calculations) and inter-layer separation = 11 μm (11.2 μm in calculations).

For the MPBG structure, the center of the second band occurs at $\lambda = 2nL$, where n is the dielectric constant of the polyimide and L is the length of the cross arm. This relationship was confirmed in another MPBG structure — lattice constant of 22 μm, line width of 1.5 μm, and cross arm length of 12.5 μm — which had the second band gap centered at 6.9 THz.

The attenuation per layer of this modified structure has also been studied. Different samples were fabricated with increasing number of metal layers. As can be seen in Fig. 20, a single layer FSS using the same pattern had a similar stopband, but the maximum rejection is only 15 dB at the center of the band. As we increased the number of layers, the attenuation in the stopband region improved. The attenuation per layer is about 15 dB. The band-edges are

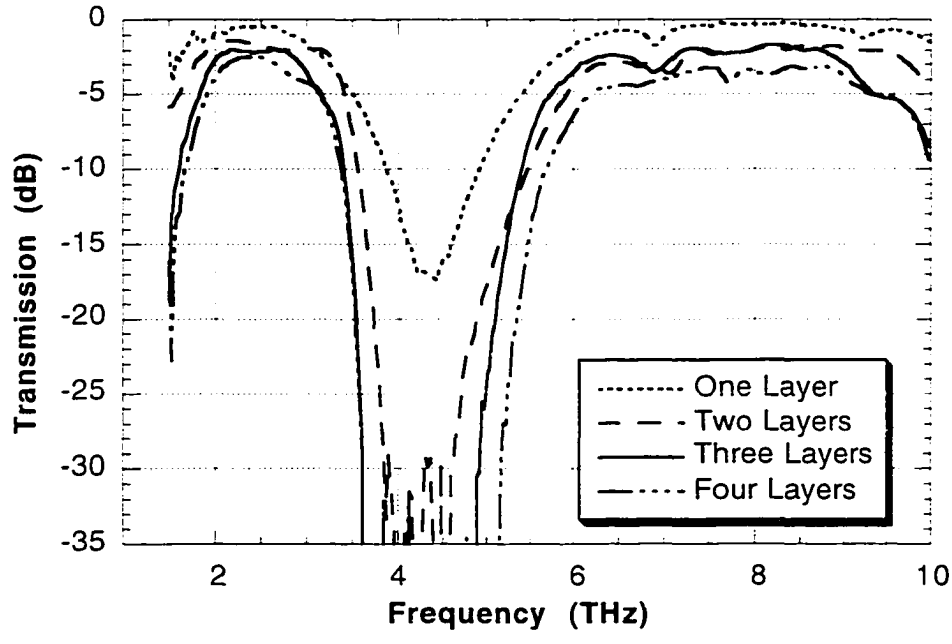

Figure 20: Transmission spectrum as a function of number of metal layers. The attenuation in higher order bandgap is 15dB/layer. Here, L = 22.5 μm, a = 16 μm, w = 2.5 μm and inter-layer separation = 11 μm.

fairly sharp for the three layer structure. The attenuation in the transmitting region suffers as we increase the number of layers. This can be attributed to absorption due to the polyimide layers.

Stopband characteristics of this band-reject structure were also studied as a function of the cross-arm length, L. It was observed that reducing the cross-arm length reduces the width of the gap, and if the cross arm length becomes too small, the second gap disappears completely. This effect can be seen in Fig. 21 which shows the transmission of three different band-reject filters with cross-arm lengths of 10.5 μm, 18.5 μm and 22.5 μm. It is also clear from the transmission results that reducing L reduces the width of the gap but increases its center frequency. The higher order bandgap almost disappears for a cross arm length of 10.5 μm.

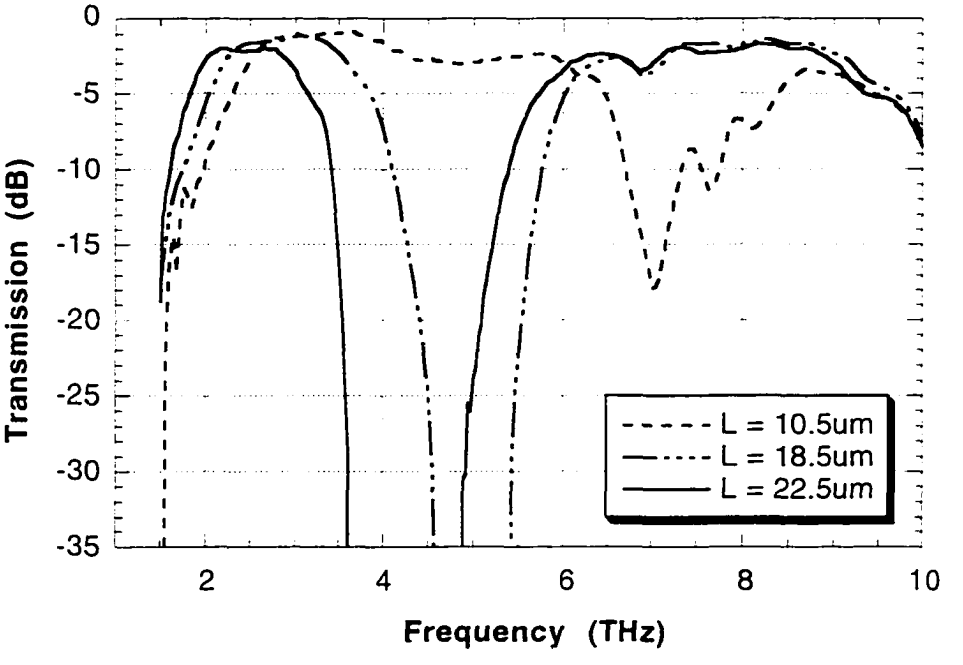

Figure 21: Change in transmission characteristic as a function of cross-arm length, L. Here, a = 16 μm, w = 2.5 μm and inter-layer separation = 11 μm.

The angular dependence of these band-reject filters were also measured. These measurement results are shown in Fig. 22 for the MPBG structure with L = 22.5 μm. The band gap is virtually independent of the angle of incidence up to 47°. Because of the limitation in sample size, measurements were not conducted for higher angles of incidence. However,

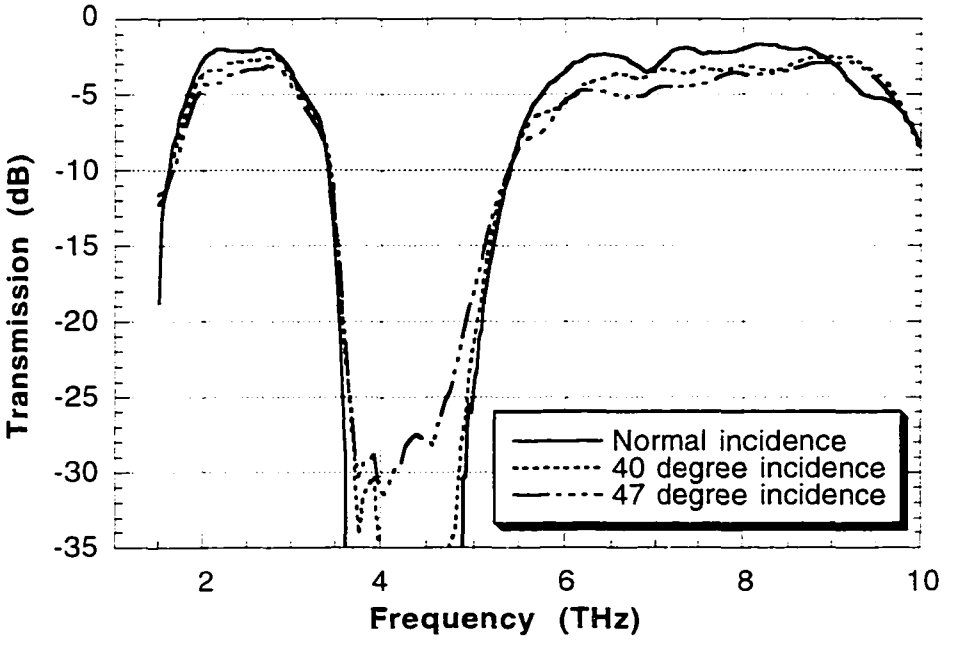

Figure 22: Angle dependence of the transmission characteristic for band-reject filter with L = 22.5 μm. Here, a = 16 μm, w = 2.5 μm and inter-layer separation = 11 μm.

theoretical calculations predict that for angles of incidence up to 80°, the transmission characteristics should not change.

All measurements for the square grid and the modified grid structures were done using an unpolarized beam. However, theoretical studies show that for normal incidence, the cutoff frequency is independent of the two polarizations. As the incidence angle increases, the

calculations show that there will be small differences between polarizations. However, even for angles as high as 80°, the difference in the cutoff frequencies of the two polarizations is less than 10%.

IV.3 FCC lattice geometry

The MPBG structures that are discussed in this section are somewhat inverse of the square grid patterns discussed in previous sections. Instead of being an array of aperture elements, these "inverse" structures are arrays of patch elements. These MPBG structures consist of arrays of square metallic patches located in a three-dimensional face-centered-cubic lattice imbedded in a flexible polyimide dielectric. The three-dimensional FCC lattice is fabricated by the same layer-by-layer technique. A top view of each layer is shown in Fig. 23. The lateral lattice constant of the array is $a_l = 20$ μm with metallic patches of 8×8 μm and metal thickness, $t_l = 0.2$ μm.

The FCC structures were fabricated using alternating layers of metal patch arrays and polyimide spacers. The first metal layer is deposited on a 5 μm polyimide layer. After depositing the 11 μm thick polyimide spacer layer the second metal patch array, shifted by half the lateral lattice constant, is deposited on the spacer. The third metal layer is aligned to the first layer to obtain the FCC crystal lattice. The unit cell size is $20 \times 20 \times 22$ μm. Fig. 24 shows the FCC lattice structure of the MPBG where the dark squares are the top and bottom layers and the middle layer is shown in the lighter shade. Several sample array of 2×2 cm were fabricated to study how the geometry affected PBG properties.

The critical frequencies of the filters depend on the lattice constant of the metallic layers and the inter-layer separation. The transmission spectrum of the FCC structure at normal

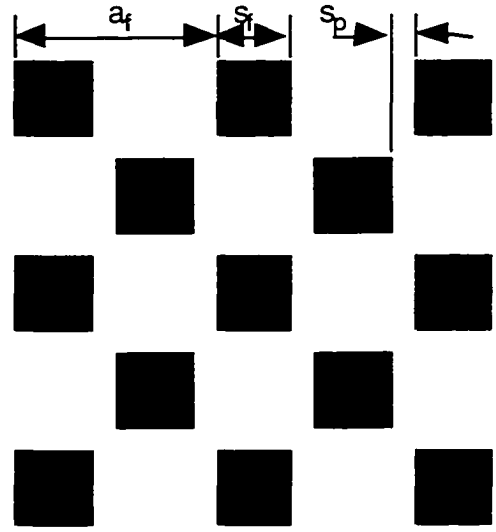

Figure 23: Top view of the square metallic patch array used for each layer to obtain the FCC or diamond lattice. Here, a_f = 20 μm, s_f = 8 μm and s_p = 2 μm

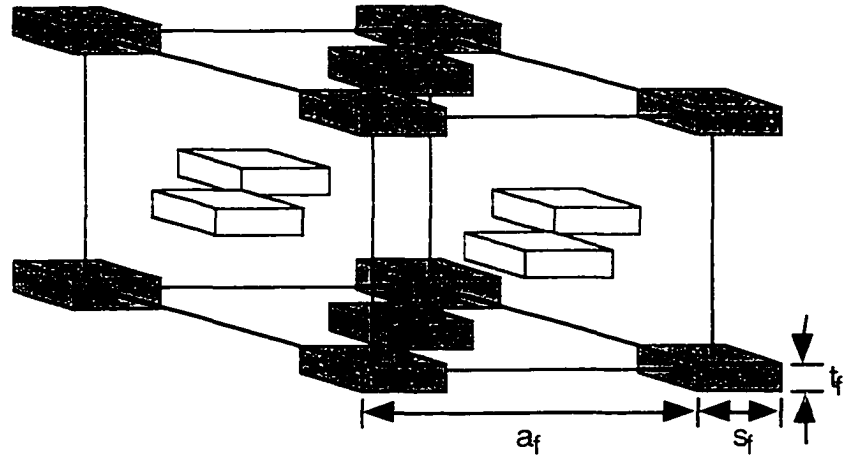

Figure 24: FCC lattice geometry with lateral lattice constant, a_f = 20 μm, metallic square patch width, s_f = 8 μm and metal thickness, t_f = 0.2 μm.

incidence is shown in Fig. 25, which shows two stopbands separated by a narrow band-pass region. The structure shows two stopbands centered around 7 and 11 THz with attenuation of more than 13 dB and 35 dB respectively. The measured values are in good agreement with predicted results. The lower pass-band region of the spectrum, below 4 THz, shows very good transmission characteristics with attenuation of only 1 dB. The reflection measurements in Fig. 25 show up to 85% reflection in the lower band gap region. The measurements shows high attenuation near 10.5 THz due to the polyimide absorption band. Both the transmission and reflection measurements are close to the predicted calculations as shown in the figure. The interference fringes due to polyimide thickness show up very clearly at the lower end of the frequency spectrum in the reflection measurements where the reflection dip between the bandgaps goes down to 25 dB between the stopbands.

Another FCC sample was fabricated with two unit cells consisting of five metal layers. Here, layers 1, 3 and 5 are aligned to each other and layers 2 and 4 are shifted by $(1/2)a_x$ in the x-axis. This sample shows the same center frequencies as the one-unit-cell structure but with much higher attenuation in the lower bandgap region, as shown in Fig. 26. The bandgap centered around 7 THz has an attenuation of more than 25 dB. The reflection measurements show that the sample is nearly 90% reflective in the lower bandgap region. Figure 26 shows the reflection and transmission curves of the two unit cell structure as compared to the one unit cell FCC characteristic. The absorption band of polyimide near 10.5 THz is very clear in the reflection measurements.

Figure 27 shows the transmission spectrum as a function of angle-of-incidence for the two-unit-cell FCC sample. With increasing incidence angle, the higher bandgap narrows and eventually disappears entirely. The narrow band-pass region between the stopbands is highly attenuated, but the lower gap remains essentially intact.

The effect of change in thickness of separation layers on the filter characteristic was also studied. Another FCC sample with an inter-layer separation of 9 μm was fabricated, and

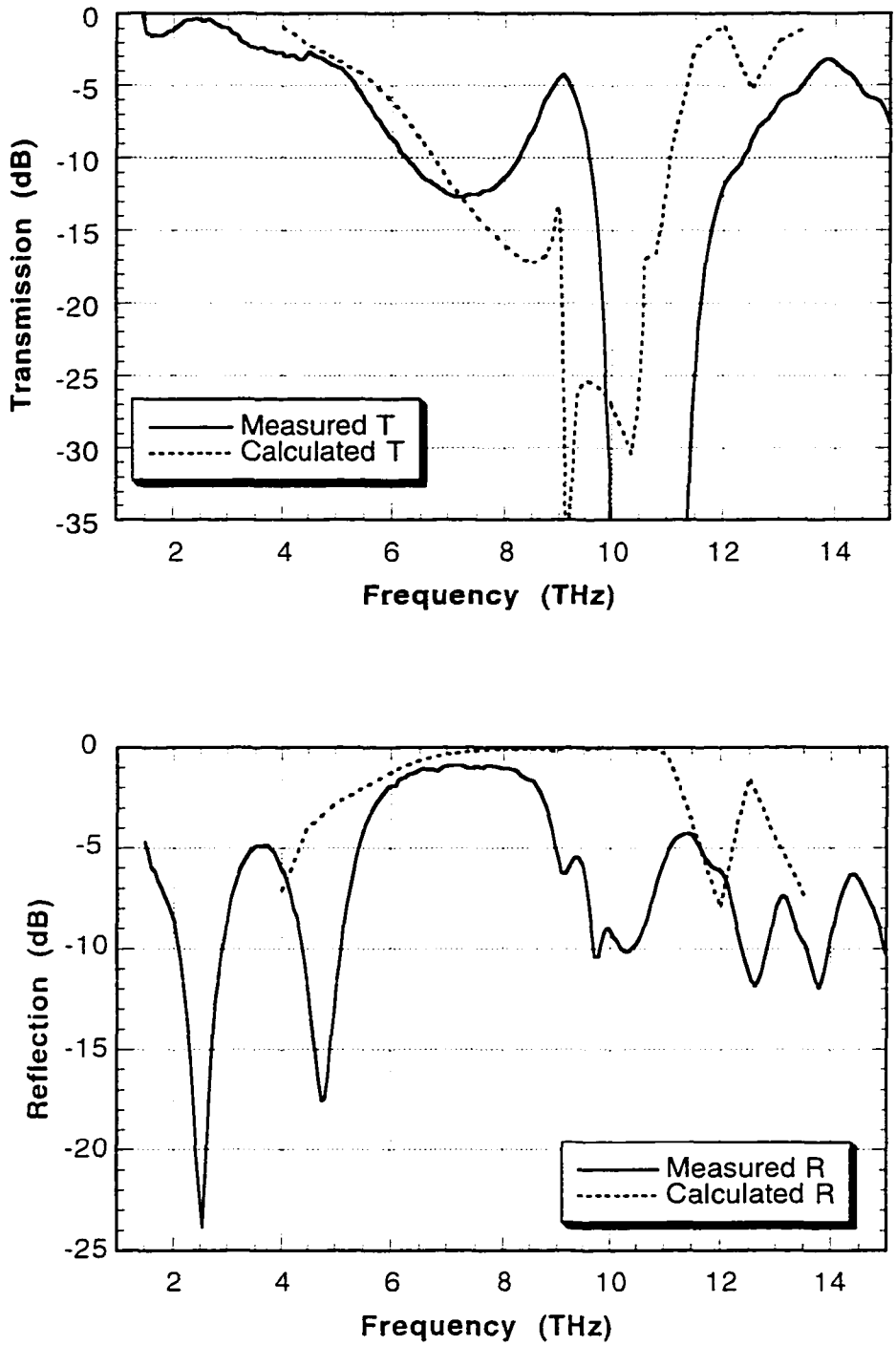

Figure 25: Transmission and reflection characteristic (measured and predicted) of a one unit cell FCC structure. Here, $a_f = 20$ μm, $s_f = 8$ μm and inter-layer separation = 11 μm.

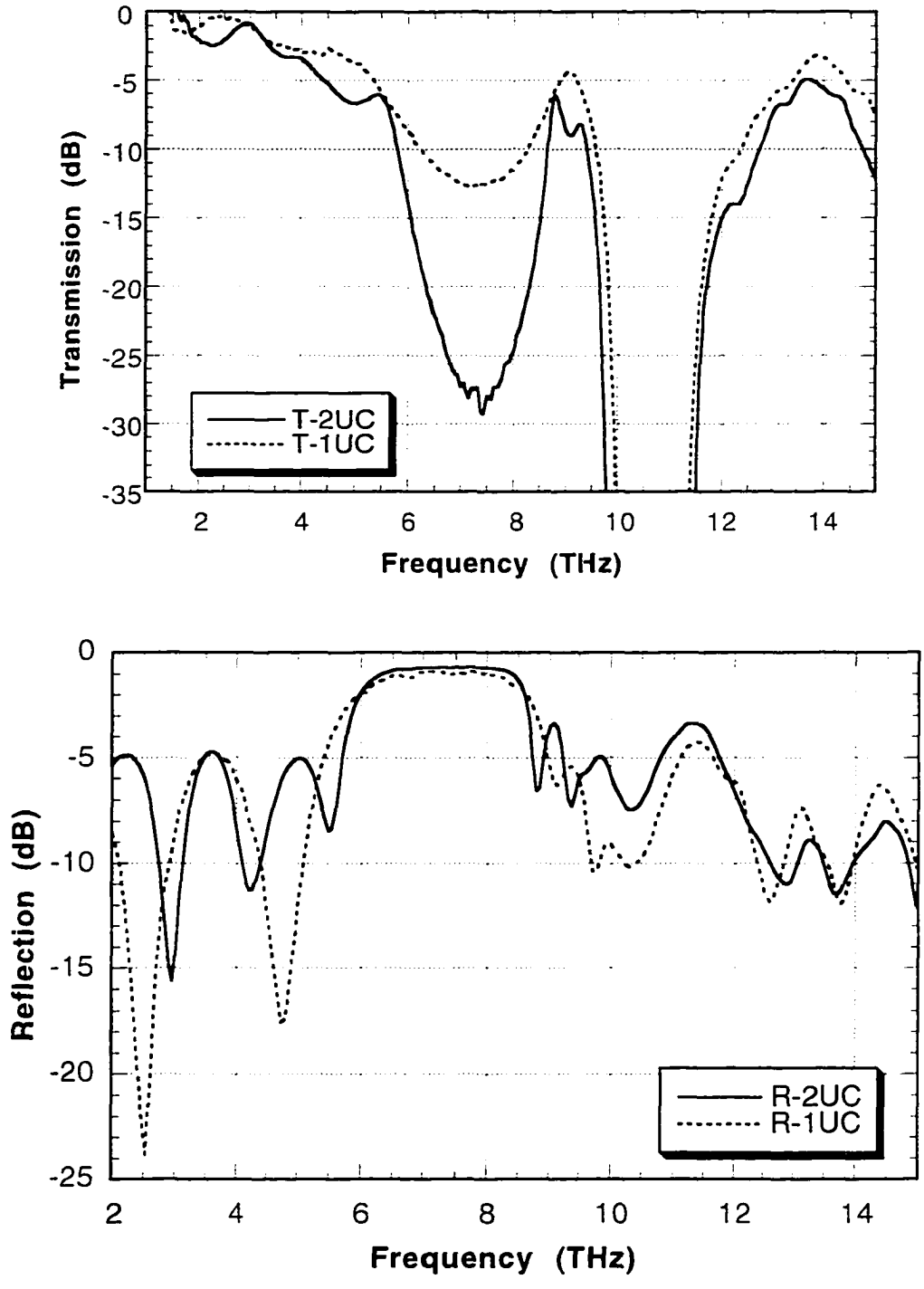

Figure 26: Comparative measurements of 1- and 2-unit cell FCC behavior. Here, a_t = 20 μm, s_t = 8 μm and inter-layer separation = 11 μm.

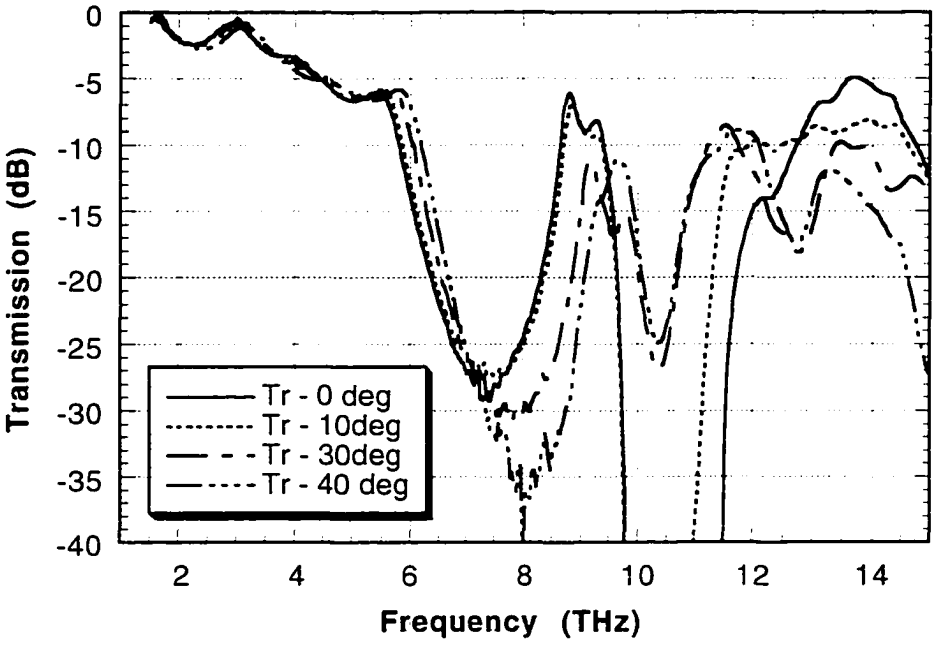

Figure 27: Angle dependence of the two unit cell FCC transmission characteristic. Here, a_f = 20 μm, s_f = 8 μm and inter-layer separation = 11 μm.

the measured characteristics are shown in Fig. 28. The theoretical results show that the narrow band-pass region between the stopbands moves to higher frequency from 9 THz to 10 THz. The measured transmission spectrum shows that the lower band edge also moves up from 5 THz to 6 THz. The narrow band pass region near 10 THz in the theoretical calculations is not visible in the measured spectrum because of the absorption peak of polyimide near 10 THz. The reflection measurement on this sample also shows very good reflectivity in the bandgap region with attenuation of only 1 dB. The polyimide absorption near 10.5 THz can be seen clearly in the reflection measurements.

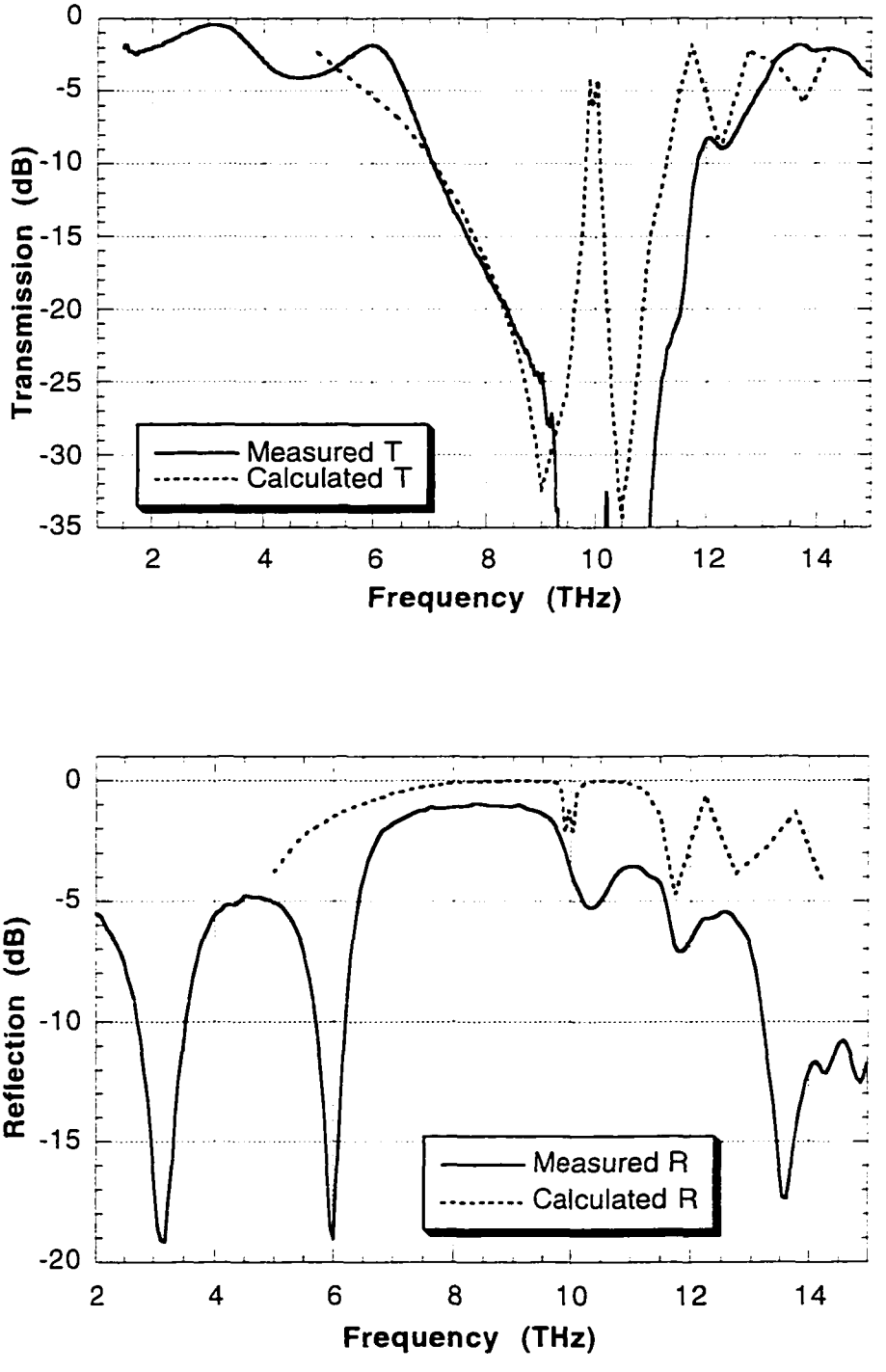

Figure 28: Measured and calculated transmission and reflection measurements on FCC sample with inter-layer separation of 9 μm. Here, a_f = 20 μm, s_f = 8 μm.

IV.4 Defect Modes in FCC

The effect of disturbing the periodicity of the FCC structure was also studied. Defects were introduced into the middle layer of a three-layer FCC structure. The defect layer is shown in Fig. 29. Here, metal square patches were removed from every other row of the periodic layer shown in Fig. 23. The blank squares represent the metal patches that are

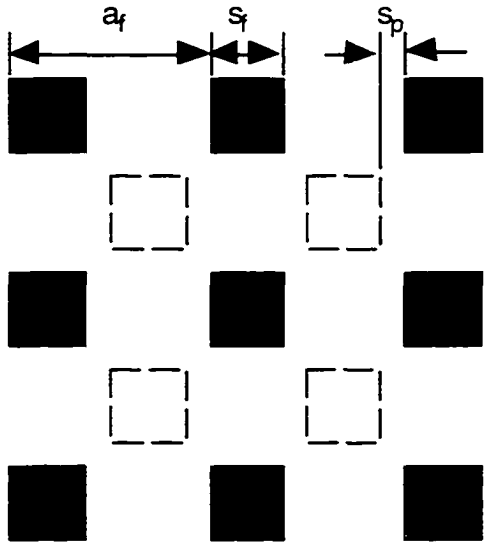

Figure 29: Defect layer (called defect "s") introduced in the middle layer of a one unit cell FCC structure. The dashed squares show the areas where metal squares have been removed.

missing in the defect layer. This defect layer is referred as defect "s" in the rest of this section.

The measured and simulated spectra for FCCs with defects are shown in Fig. 30. The calculations predict the presence of multiple defect peaks on the low frequency side of the band gap. However, only a single defect peak near 7.7 THz can be seen in the measurements.

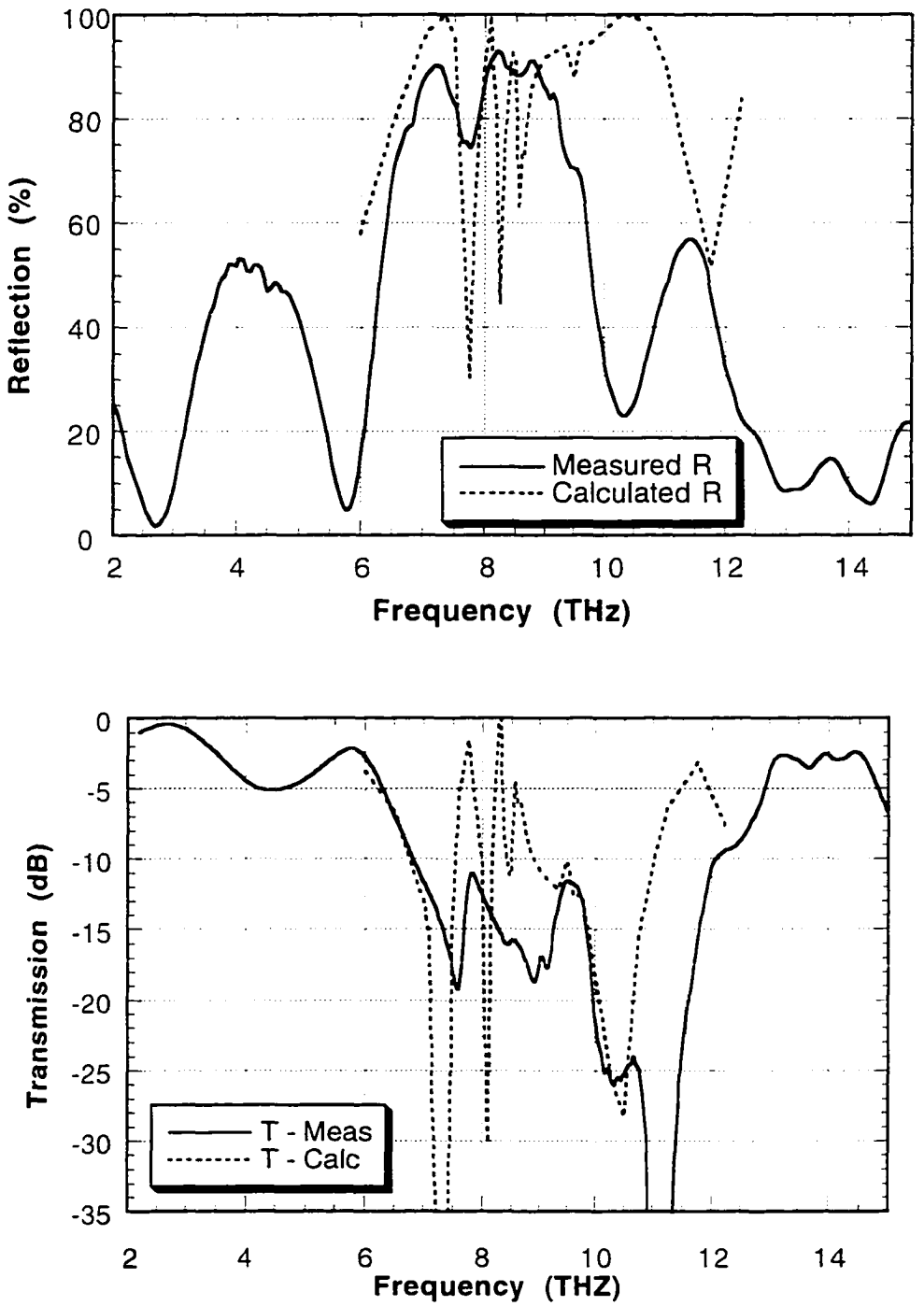

Figure 30: Measurements and calculation results when a defect is introduced in the middle layer of one unit cell FCC. Here, a_f = 20 μm, s_f = 8 μm and inter-layer separation = 11 μm.

This is the strongest peak in the measured spectrum, showing a reflection dip down to 75% and transmission peak intensity of -11 dB. The other defect peaks are highly attenuated. This may be due to polyimide absorption.

The defect peak intensity is not very strong in the measurements shown in Fig. 30. In an effort to improve the defect peak intensity, one of the inter-layer separations was changed. MPBG structures were fabricated which not only contain defect patterns in the middle layer as shown in Fig. 31, but also have defects introduced by altering the separation between the middle and the top metal layer, $t_{m\text{-}t}$. Different samples were fabricated with varying $t_{m\text{-}t}$ as shown in Table 3.

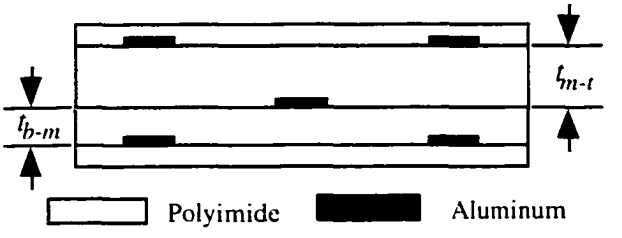

Figure 31: Cross-section of a unit cell of face-centered-cubic lattice with defect layer in the middle and variable inter-layer separation, $t_{m\text{-}t}$.

Here, $t_{b\text{-}m}$ is the inter-layer separation between the bottom and the middle metal patch arrays and $t_{m\text{-}t}$ is the inter-layer separation between the middle and the top metal patch array. All the samples have a top and bottom coating of 5 μm thick polyimide. Figure 32 shows the measurement results of defect structures with varying values of $t_{m\text{-}t}$. The measurements shown in Fig. 31 were taken with top layer side of the sample facing the incident beam. Figure 32 shows that reducing $t_{m\text{-}t}$ increases the peak intensity of the defect mode. The transmission spectrum shows that the defect peak intensity attenuation near 8 THz

Table 3: Different inter-layer separations used for FCC structures with defect metal patch array introduced in the middle layer. The samples have a_f = 20 μm, s_f = 8 μm and the defect layer "s" as shown in Fig. 29.

Sample No.	$t_{b\text{-}m}$ (μm)	$t_{m\text{-}t}$ (μm)
X	11	20
Y	11	11
Z	11	5

improves from 17 dB for 20 μm separation to 3 dB for 5 μm separation. The Q value of the defect peak also improves significantly.

The reflection measurements on these samples also show the best reflection dip for the inter-layer separation, $t_{m\text{-}t}$ = 5 μm with attenuation of about 8.5 dB near 8 THz. The graph shows that the lower band-edge of the structure moves to a higher frequency by both reducing or increasing the periodic inter-layer separation between the metal patch arrays.

The reflection measurements are sensitive to the sample surface which is closer to the incident beam. For samples with differing inter-layer separations, it was observed that the band-edge attenuation and the defect frequency attenuation are better when the samples are oriented so that the thinner separation layer is closer to the incident beam. The reflection measurements in Fig. 33 show that the defect peak intensities are significantly reduced for sample Z when the sample is flipped. The transmission measurements are not dependent on the sample side on which the beam is incident.

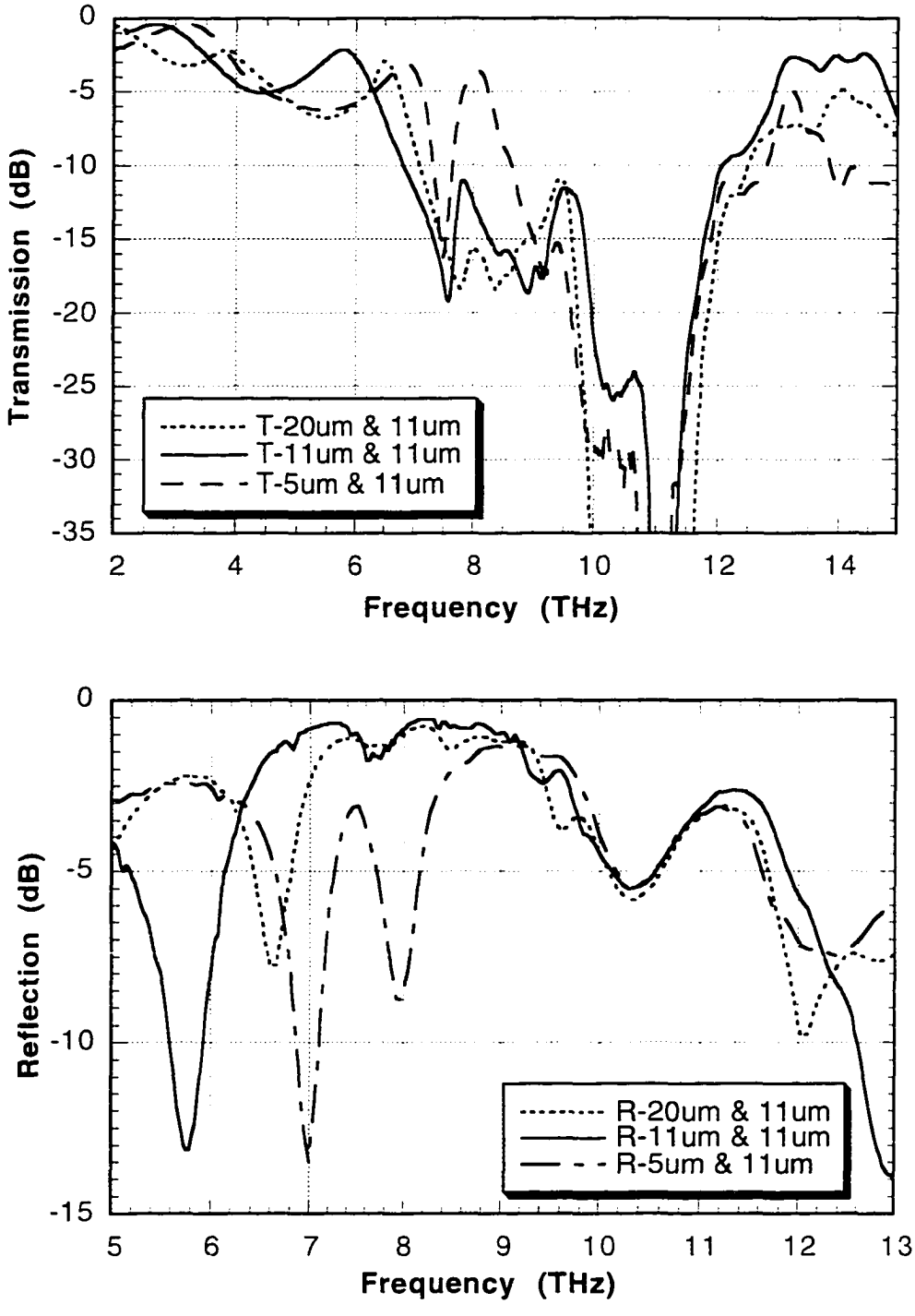

Figure 32: Measurement on FCC defect structures as a function of varying separations. The first number on the graph labels indicate the inter-layer separation closer to the incoming beam.

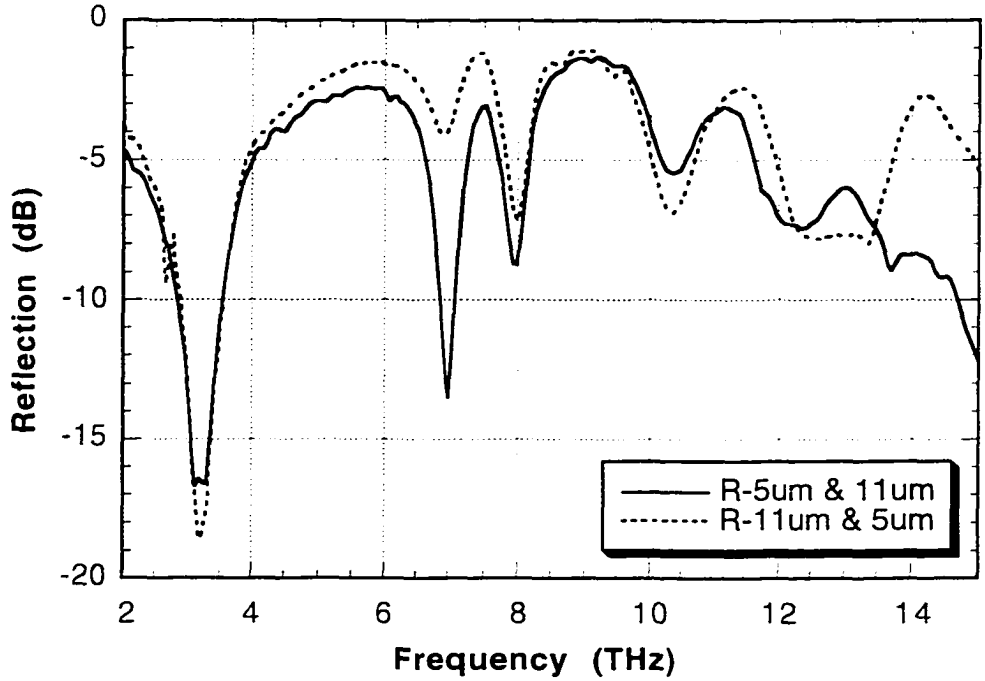

Figure 33: Reflection measurement done on both sides of the sample Z. The first set of numbers on the graph labels indicate the inter-layer separation that is facing the incoming beam.

One more set of structures was studied with defect layer patterns having metal squares removed from every fourth row. This defect pattern is referred as defect "o" in the rest of this section. For these samples, the defect layer was the middle layer of the MPBG structure, and the inter-layer separations are same as sample set Z, i.e. 11 μm and 5 μm. The measurements were taken with the 5 μm separation layer closer to the incoming beam. The defect frequency in the transmission and reflection measurement on these samples show less attenuation levels than the defect peak measurements on samples with defect "s". As shown in Fig. 34, the defect peaks in the "o" sample have been almost completely smeared out - the perturbation to the periodicity is too weak to create a strong defect resonance.

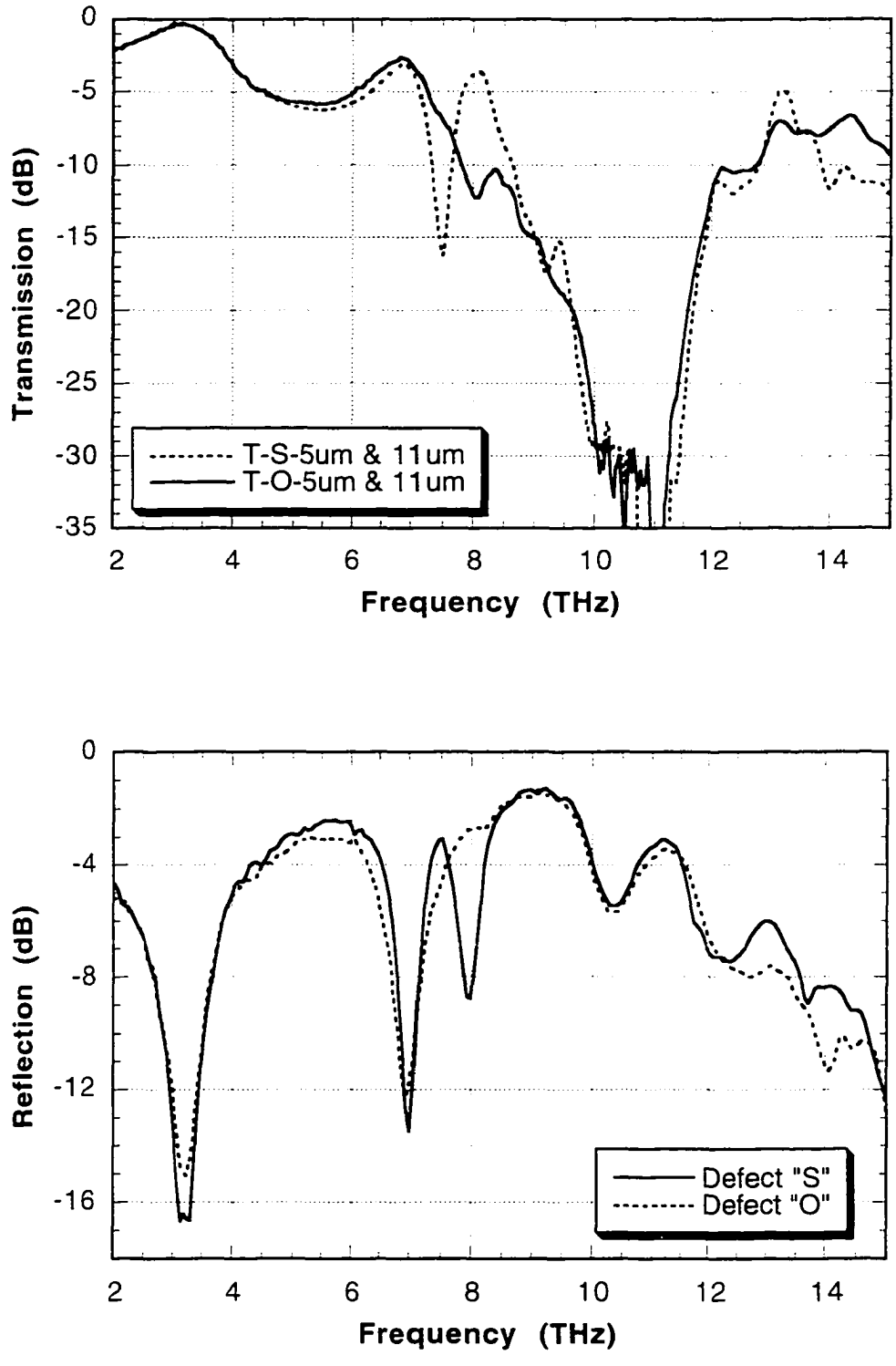

Figure 34: Measurements on FCC defect structures with defects "s" and "o".

IV.5 Diamond lattice geometry

Diamond lattice geometries were also studied. The fabrication strategy is unchanged. The diamond lattice requires five metal layers to form a unit cell, with each metal layer being shifted by $(1/4)a_f$ in x- and y- directions relative to its adjacent layers. This process is repeated up to the fifth layer which is aligned to the first metal layer. The same metal mask used for FCC is utilized for fabrication of diamond lattice also. The separation layers for the diamond lattice were each 5 μm thick, leading to a unit cell size of 20 × 20 × 20 μm.

The measured and calculated spectra for the diamond structure are shown in Fig. 35. The transmission spectrum shows a bandgap from 8.5 to 12.5 THz with an attenuation of more than 35 dB in the bandgap. The calculated results are close to the measurements. In the diamond structure the transmission does not recover very well near the higher edge of the bandgap as compared to an FCC structure and shows an attenuation of more than 10 dB in the transmitting region. The reflection spectrum reaches up to 90% (< 1 dB) in portion of the bandgap region. The attenuation near the 10 THz region is due to the characteristic absorption peak of the polyimide.

IV.6 Observations on the mechanical properties of flexible MPBG structures

All the metallic PBG structures discussed in this work maintain their transmission and reflection properties after considerable mechanical flexing. The structures were repeatedly rolled into a 8 mm diameter cylinder and then unrolled. No measurable changes in the transmission and reflection characteristics were observed after flexing the structure.

Rapid cooling of the samples also does not show any visible stress on the sample. Samples were dipped in liquid nitrogen and left there for 15 minutes. There were no observable

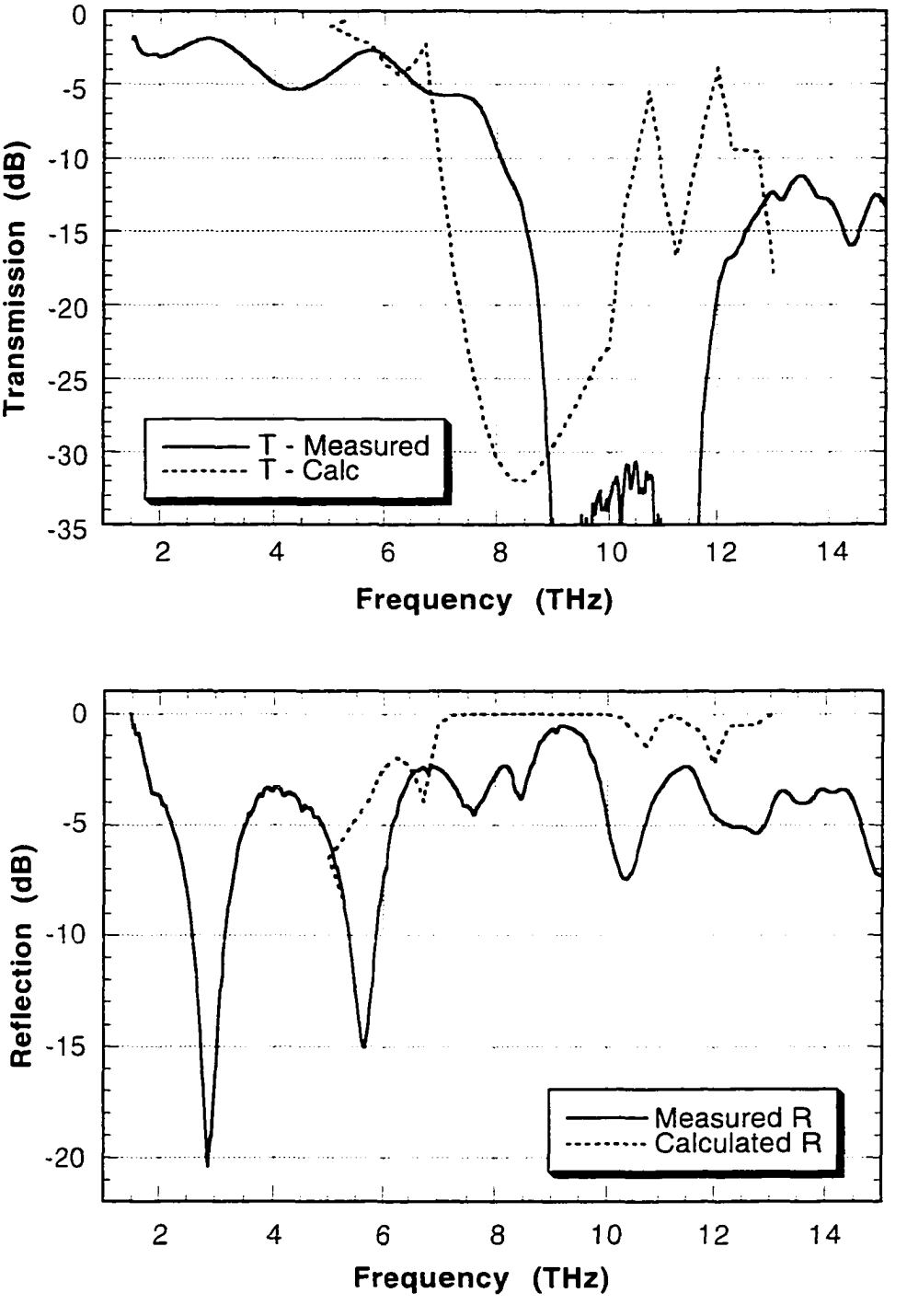

Figure 35: Measurements and calculations for the diamond lattice geometry. Here, $a_f = 20$ μm, $s_f = 8$ μm and inter-layer separation = 5 μm.

cracks or other form of visual damage. The optical properties of the sample also did not change after the rapid temperature changes. This behavior makes these MPBG structures an excellent candidate for space applications.

The samples are very light-weight and compact. The characteristics of the structure do not change over a period of time. Measurements on a sample structure were taken after 18 months and it did not show any change in its characteristics.

IX. CONCLUSION

Flexible metallic PBG filter structures operating at far-infrared frequencies have been designed, fabricated and characterized. The MPBGs have a simple, microfabrication-based construction that uses alternating dielectric and metal layers and results in structures that are mechanically flexible. The structures can be fabricated by one person in about 4-5 days using well known technologies and equipment readily available at most semiconductor research facilities. The performance of the structures are in good agreement with theoretical predictions, within the limits stated earlier.

High-pass structures show cutoff in the far-infrared region with very good attenuation (>35 dB) in the stopband region. The cutoff frequencies of the structures are a function of the dielectric constant of the polyimide, lattice constant of the metal grid and the inter-layer separation between the metal layers. By introducing a defect in the middle layer of the structure, a defect peak has been created in the stopband region. The frequency of the defect peak is a function of the defect size.

Band-reject filters show higher order gaps in addition to the lower bandgap region present in the high-pass structure. This higher order bandgap is a function of the metal bars sitting at the cross arms of the structures. It shows high attenuation level as good as the high-pass structure. The filter characteristics are relatively independent of the angle of incidence measured up to 50°.

Face-centered-cubic and diamond crystal lattices show a fundamentally different stopband behavior as compared to the interconnected metallic structures. These crystal geometries show very good reflection characteristic in the bandgap region with reflections of nearly 90% in FCC case. The critical frequencies are a function of lattice constant and the inter-layer separations. Defect peaks can be created in the bandgap region by introducing defect in the middle layers of the FCC or diamond structures.

The filters maintain their optical characteristics after repeated bending, demonstrating mechanical robustness of the MPBG structure. Rapid cooling of the samples in liquid nitrogen also does not show any visible stress on the sample or its optical characteristics making them excellent candidates for space applications.

X. FUTURE WORK

The structures show very good attenuation in the band-stop regions, but in the transmitting region they tend to show an attenuation of 1-3 dB, i.e. up to 50% of the signal is sometimes lost in the transmitting region. The structures show highly attenuated defect peaks and relatively poor Q values. This is mainly due to the absorption in polyimide. One way to achieve better Q is to etch polyimide from the areas between the metallic grid. This would effectively reduce the polyimide absorption effect and result in better Q for the defect peaks. The reactive ion etching of polyimide needs to be studied in detail.

These structures might have possible applications in infrared astronomy. The recently acquired funding for this project through the Iowa Space Grant Consortium has given a great opportunity to pursue the possible use of MPBG structures in the area of infrared astronomy. Similarly strong effort needs to be directed in finding other applications for the flexible metallic structures.

The infrared filters presently available via other technologies are bigger and bulkier as compared to these flexible metallic filters. However, they have the advantage of having tunable filter characteristics. Possible ways of tuning these filters need to be studied in detail. One possible avenue towards tunability is to use two FCC structures in the form of Fabry-Perot resonators where the separation distance between the filters can be fine tuned using semiconductor micromachining techniques.

Although filters operating in the far IR (near 100 μm wavelength) have been demonstrated, the structural dimensions could easily be scaled down to work at much higher frequencies, providing that a suitable low-absorption dielectric can be used. Polyimide has very strong absorption band from 15 to 54 THz, although it would also be suitable for applications at higher frequencies. MPBG structures operating in this mid-infrared region may need much finer metal linewidths. This will put a premium on fabrication capabilities.

APPENDIX I: POLYIMIDE PROCESSING

The processing steps for obtaining a polyimide layer of desired thickness are listed here. The desired thickness of polyimide can be achieved by controlling its spin speed. Desired thickness vs spin speed plot is shown in Fig. 36. This process can be used for obtaining a maximum thickness of 11μm for a cured polyimide layer.

Process Steps:

1.	Dehydration bake	130°C	30 mins.
2.	Spread	500rpm	5 sec.
3.	Spin	Depends on desired thickness	45 sec.
		(See figure)	
4.	Softbake	130°C	30 mins.
5.	Cure	Push at 200°C	
		Ramp up 350°C	_____
		Soak at 350°C	30 mins.
		Ramp down 200°C	_____
		Pull	
6. Measure polyimide thickness			_____ μm

For obtaining polyimide layers thicker than 11 μm, multiple coats may be used. The process steps remain the same as for a single layer of polyimide up to the softbake step for the first layer. Another polyimide layer is spun on after it and softbaked. The sample is now ready for the final cure. For multiple coats the thickness vs spin speed graph will not be valid.

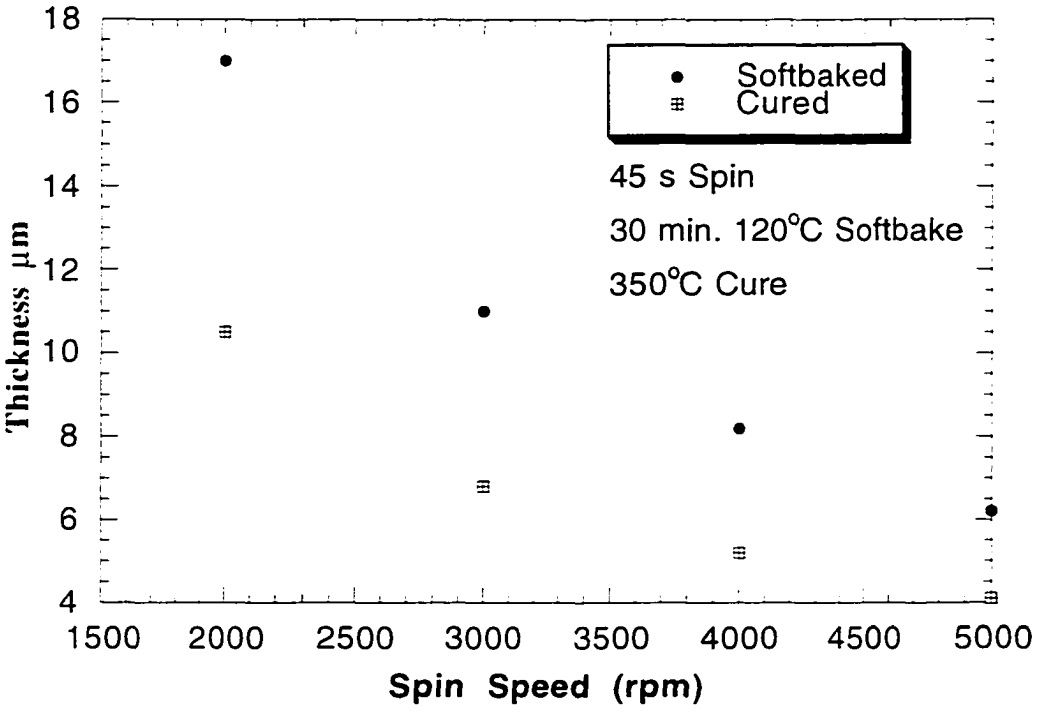

Figure 36: Softbake and cured polyimide thickness as a function of spin speed.

APPENDIX II: METAL LIFT-OFF PROCESS

The recipe for obtaining a metal pattern using the lift-off processing technique are listed here. Photoresist AZ 5209E has been used for masking which gives a thickness of about 1 μm for spin speed of 3000 rpm. Aluminum is deposited by e-beam evaporation. Figure 37 shows the various processing steps involved to obtain a metal pattern on the wafer.

Process steps:

1.	Dehydration bake	120°C	30 mins.
2.	Spin photoresist	3000 rpm(AZ 5209E)	45 seconds
3.	Postbake	90°C	30 mins.
4.	Align and Expose		75 seconds
5.	Chlorobenzene soak		10 mins.
6.	Develop	AZ312	_____ mins.
7.	E-beam evaporation	Aluminum	2000 Å
8.	Metal lift-off	Acetone	_____ mins.
		(Use ultrasonic stirrer)	

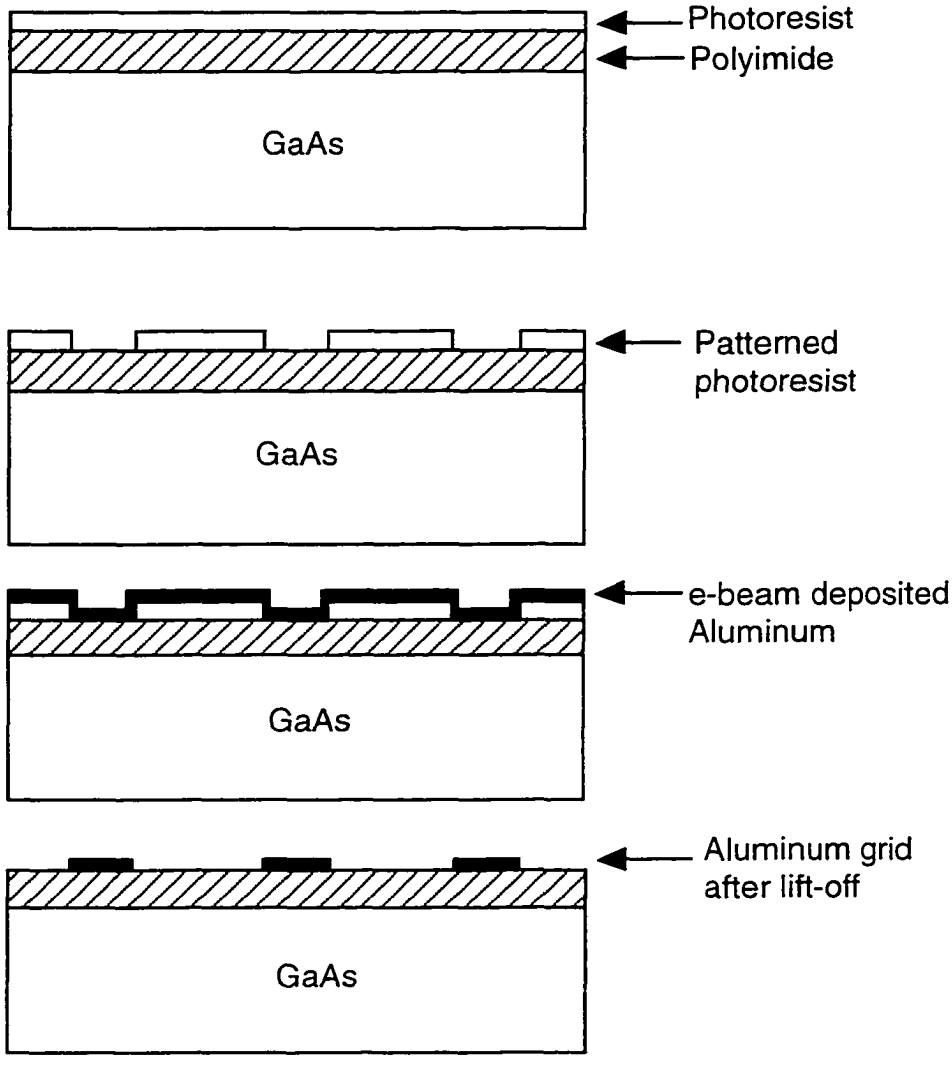

Figure 37: Processing steps for depositing a single layer of metallic aperture or patch arrays

APPENDIX III: FOURIER TRANSFORM INFRARED SPECTROMETER

Figure 38 shows the basic FTIR setup in which the infrared light from the source "A" is incident on the Michelson interferometer, the main component of FTIR spectrometry. The interferometer modulates each wavelength of light at a different frequency.

The light beam from the source strikes the beamsplitter(B), of which about half is reflected from B and is directed to the fixed mirror C. The remaining light is transmitted through the beamsplitter and is directed onto the moving mirror, D. When the two beams recombine, constructive or destructive interference occurs depending on the position of the moving mirror relative to the fixed mirror.

The modulated beam is reflected from mirror to the sample, where selective absorption takes place. The beam travels from the sample on to the detector which translates it to an electrical signal.

The cosine waves produced by the source and modulated by the interferometer appear to the detector as an interferogram. This is a signature of intensity versus mirror position. The interferogram is a summation of all the IR frequencies and cannot be interpreted in its original form for all practical purposes. The signal from the detector is fourier transformed by the computer and converted into an IR spectrum. Fourier Transform calculates the amplitude of each of the component signals which gives the intensity at the corresponding wavelength of light.

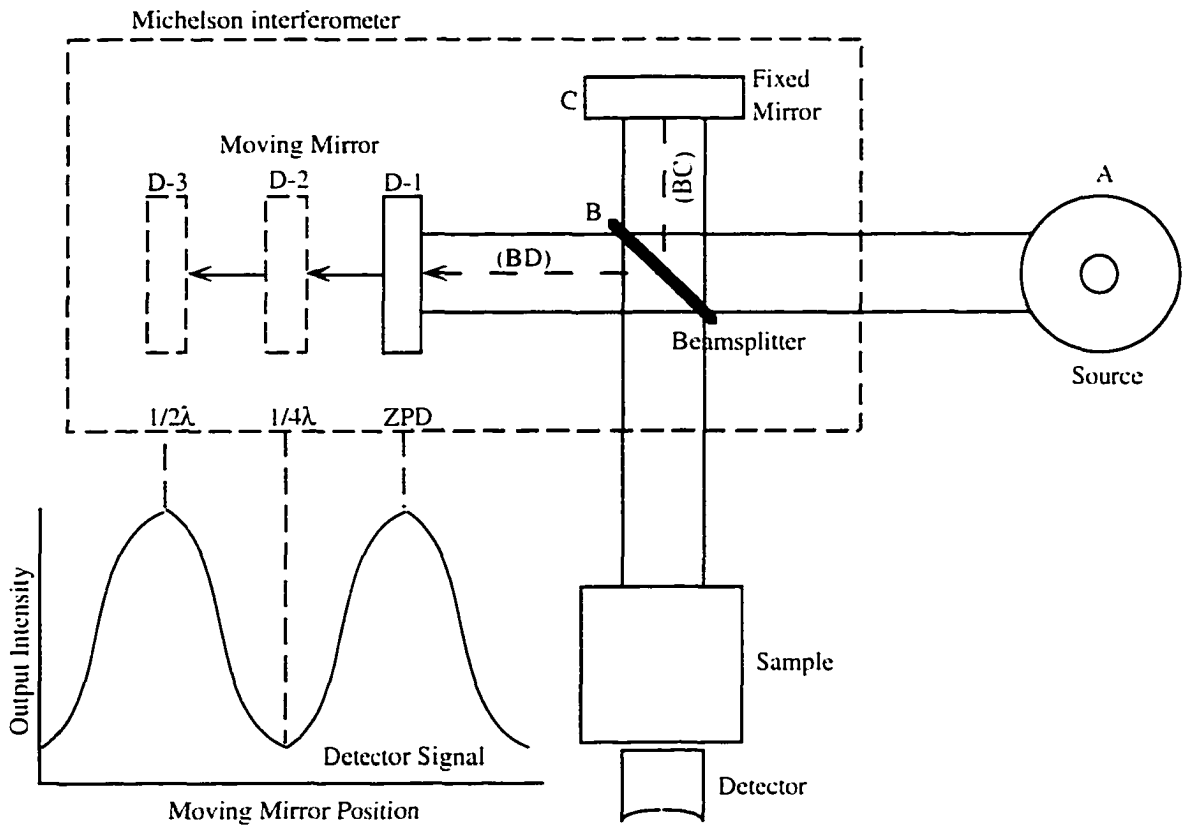

Figure 38: FTIR Spectrometer setup with source (A), beamsplitter (B), fixed mirror (C), moving mirror (D) at positions D-1, D-2 and D-3. The graph on the lower left hand corner shows the output intensity as a function of mirror position for a single wave length.[26]

REFERENCES

[1] E. Yablonovitch, "Inhibited Spontaneous Emission in Solid State Physics and Electronics", Physics Review Letters , vol. 58, pp. 2059-2062, 1987.

[2] See review articles, Journal of Optical Society of America B , vol. 10, 1993.

[3] Joannopoulos, J. D., Meade, R. D., Winn, J. N., "*Photonic Crystal: Molding the Flow of Light*", Princeton University Press, Princeton, New Jersy, 1995.

[4] E. Yablonovitch, Gmitter, T. J., "Donor and Acceptor Modes in Photonic Band Structure," Physics Review Letters , vol. 67, pp. 3380-3383, 1991.

[5] A. A. Maradudin, McGurn, A. R., "Photonic band structures of two-dimensional dielectric media," Physics Review B , vol. 48, pp. 17576, 1993.

[6] R. D. Smith, Schultz, S., Kroll, N., Sigalas, M., Ho, K. M., Soukoulis, C. M., "Experimental and theoretical results for a two-dimensional metal photonic band-gap cavity," Applied Physics Letters , vol. 65, pp. 645-647, 1994.

[7] M. M. Sigalas, Chan, C. T., Ho, K. M., Soukoulis, C. M., "Metallic photonic band-gap materials," Physical Review B , vol. 52, pp. 11744-11751, 1995.

[8] E. R. Brown, McMahon, O. B., "Large electromagnetic stop bands in metallodielectric photonic crystals," Applied Physics Letters , vol. 67, pp. 2138-2140, 1995.

[9] T. K. Wu, "*Frequency Selective Surface and Grid Array*",John Wiley and Sons, Inc., New York, 1995.

[10] T. Schimert, Koch, M.E., "Analysis of scattering from frequency-selective surfaces in the infrared," Journal of Optical Society of America A , vol. 7, pp. 1545-1553, 1990.

[11] P. G. Huggard, Meyringer, M., Schilz, A., Goller, K., Prettl, W., "Far-infrared bandpass filters from perforated metal screens," Applied Optics , vol. 33, pp. 39-41, 1994.

[12] K. M. Ho, Chan, C. T. and Soukoulis, C. M., "Existence of Photonic Band Gap in Periodic Dielectric Structures," Physics Review Letters , vol. 65, pp. 3152-3155, 1990.

[13] E. Yablonovitch, Gmitter, T. J., Leung, K. M., "Photonic Band Structure: The Face-Centered-Cubic Case Employing Nonspherical Atoms," Physical Review Letters , vol. 67, pp. 2295-2298, 1991.

[14] C. C. Cheng, Arget-Engels, V., Scherer, A., Yablonovitch, E., "Nanofabricated three dimensional photonic crystal operating at optical wavelengths," Physica Scripta , vol. T68, pp. 17-20, 1996.

[15] K. M. Ho, Chan, C. T., Soukoulis, C. M., Biswas, R. and Sigalas, M., "Photonic Band Gaps in Three Dimensions: New Layer-by-Layer Periodic Structures," Solid State Communications , vol. 89, pp. 413-416, 1994.

[16] E. Ozbay, Abeyta, A., Tuttle, G., Tringides, M., Biswas, R., Chan, C. T., Soukoulis, C. M., Ho, K. M., "Measurement of a three-dimensional photonic band gap in a crystal structure made of dielectric rods," Physical Review B , vol. 50, pp. 1945-1948, 1994.

[17] E. Ozbay, Michel, E., Tuttle, G., Biswas, R., Sigalas, M., Ho, K. M., "Micromachined millimeter-wave photonic band-gap crystals," Applied Physics Letters , vol. 64, pp. 2059-2061, 1994.

[18] M. C. Wanke, Lehmann, O., Muller, K., Wen, Q., Stuke, M., "Laser rapid prototyping of photonic band gap microstructures," in Science vol. 275, , 1997, pp. 1284-1286.

[19] D. F. Sievenpiper, Sickmiller, M. E., Yablonovitch, E., "3D Wire Mesh Photonic Crystals," Physical Review Letters , vol. 76, pp. 2480-2483, 1996.

[20] J. S. McCalmont, Sigalas, M. M., Tuttle, G., Ho, K.-M., Soukoulis, C. M., "A layer-by-layer metallic photonic band-gap structure," Applied Physics Letters , vol. 68, pp. 2759-2761, 1996.

[21] S. Gupta, Tuttle, G., Sigalas, M. M., Ho, K.-M., "Infrared filters using metallic photonic band gap structures on flexible substrates," Applied Physics Letters , vol. 71, pp. 2412-2414, 1997.

[22] K. A. Mcintosh, Moaoney, L. J., Molvar, K. M., McMohan, O. B., Verghese, S., Rothchild, M., Brown, E. R., "Three-dimensional metallodielectric photonic crystals exhibiting resonant infrared stop bands," Applied Physics Letters , vol. 70, pp. 2937-2939, 1997.

[23] D. W. Porterfield, Hesler, J. L., Densing, R., Mueller, E. R., Crowe, T. W., Weikle II, R. M., "Resonant metal-mesh bandpass filters for the far infrared," Applied Optics , vol. 33, pp. 6046-6052, 1994.

[24] J. B. Pendry, MacKinnon, A., "Calculation of Photonic Dispersion Relations," Physics Review Letters , vol. 69, pp. 2772-2775, 1992.

[25] E. Ozbay, Tuttle, G., Sigalas, M., Soukoulis, C. M., Ho, K. M., "Defect structures in a layer-by-layer photonic band-gap crystal," Physical Review B , vol. 51, pp. 13961-13965, 1995.

[26] "*Magna-IR FT-IR Spectromenter: System 560 and 760 User's Guide*", Nicolet Instrument Corporation, Madison, WI, 1996.

ACKNOWLEDGMENTS

I would like to take this opportunity to thank Dr. Gary Tuttle for his guidance and assistance on this project. I would also like to thank Gary for giving me the option to pursue this project which has proven to be very interesting and quite rewarding.

My special thanks to my committee members: Dr. Kai-Ming Ho for his insightful discussions, Dr. William C. Black for his encouragement and support, Dr. Robert Weber for guiding me not only for my Master's work but also serving on my Ph. D. committee and Dr. Rana Biswas for his information on all the different structures available at this time. My special thanks to Mike Sigalas for doing all the theoretical calculations for these structures that I have fabricated. Also, thanks Mike for all those long discussion about these structure and their physics.

I would also like to thank all my friends and colleagues at Microelectronics Research Center, Shi-Di Cheng, Jonathan Kavanaugh, Jennifer Dolan, Wai Leung, Russ, Phillip, Karl, Jason, Gary Knaus and Ruth Shinar and all others who made the working environment more enjoyable.

IMAGE EVALUATION TEST TARGET (QA-3)

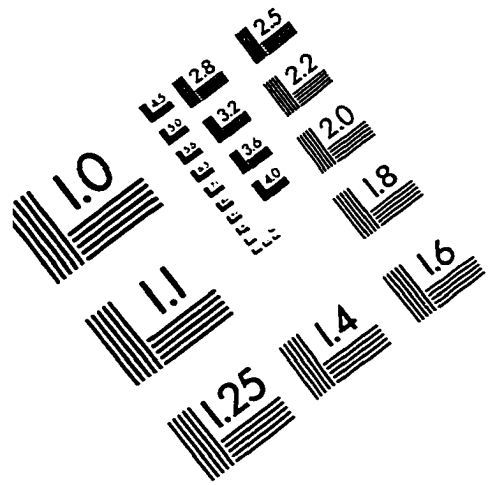

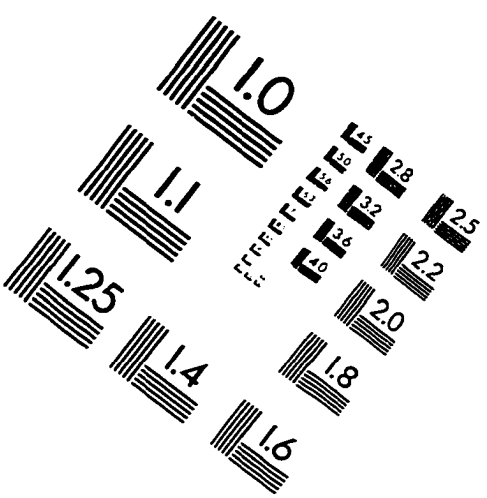

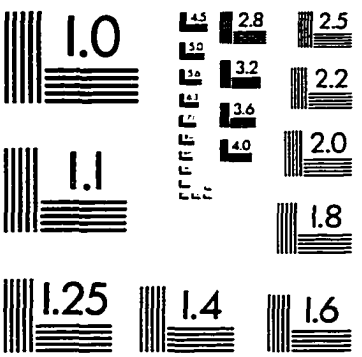

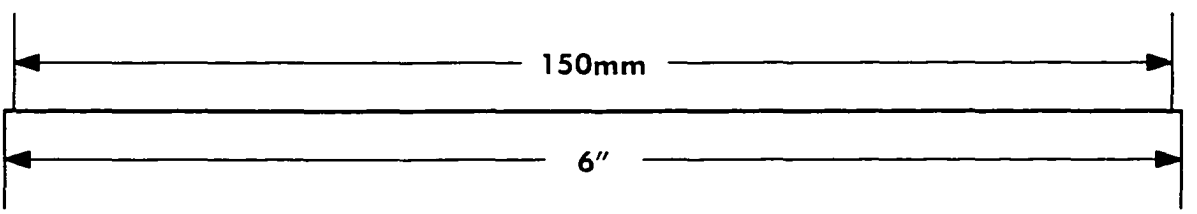

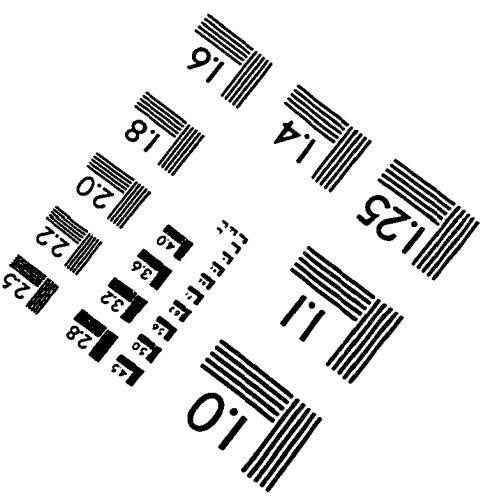

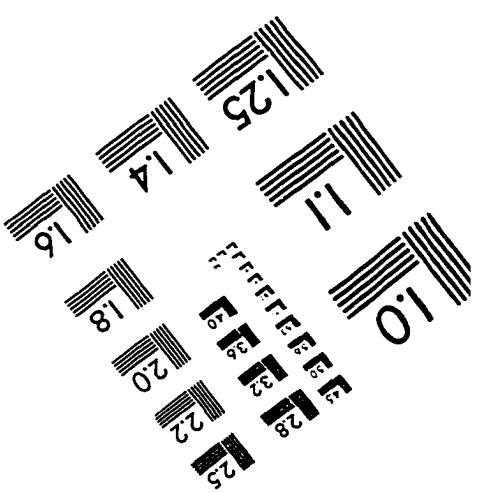

APPLIED IMAGE, Inc
1653 East Main Street
Rochester, NY 14609 USA
Phone: 716/482-0300
Fax: 716/288-5989